جامعة الملك عبدالله
للعلوم والتقنية
King Abdullah University of
Science and Technology

UK Consortium on Turbulent Reacting Flows
Annual Meeting 2022
September 13-14
Newcastle University

Hydrogen and Ammonia Turbulent Premixed Combustion: Physical Characteristics and Computational Implications

Hong G. Im
Professor in Mechanical Engineering
Clean Combustion Research Center (CCRC)
King Abdullah University of Science and Technology (KAUST)

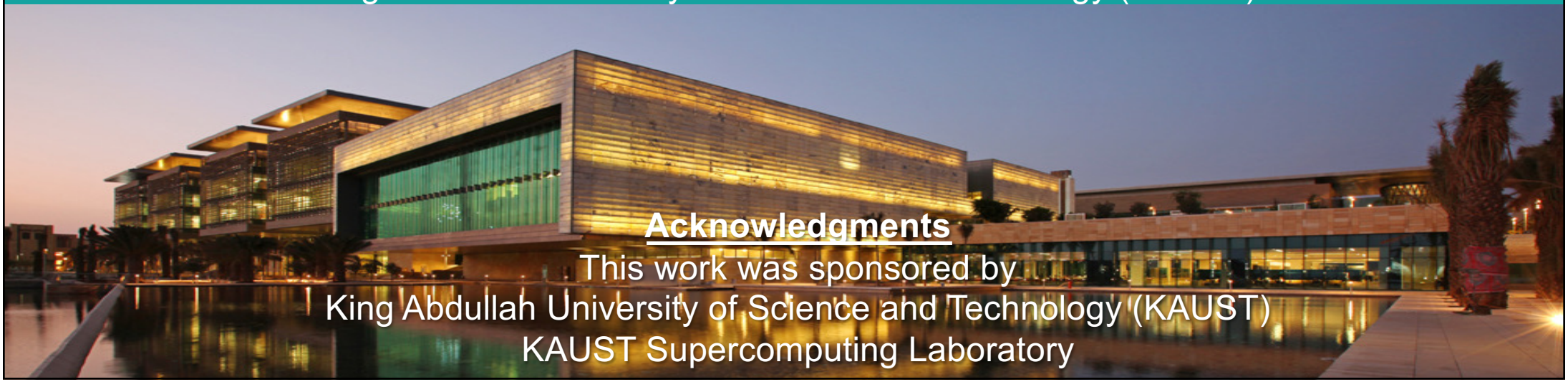

Acknowledgments
This work was sponsored by
King Abdullah University of Science and Technology (KAUST)
KAUST Supercomputing Laboratory

Computational Reacting Flows Laboratory (CRFL)
Personnel (25 members, 14 countries)

Hong G. Im
Principal Investigator

Francisco Hernández Pérez
Research Scientist

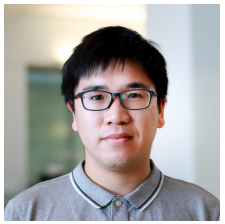

Junjun Guo
Research Scientist

Postdocs

Minh Bau Luong

Xinlei Liu

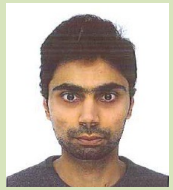

Mohammad
Rafi Malik

Jiabo Zhang

M.S. Students

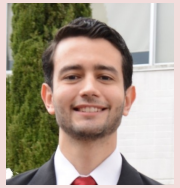

Urbano
Medina Martinez

Rafael
Menaca Cabrera

Iliana Dimitrova

Ph.D. Students

Sangeeth Sanal

Erica Quadarella

Alberto Ceschin

Moaz Lehaibi

Hammam Aljabri

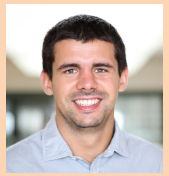

Lorenzo
Angelilli

Juan
Restrepo Cano

Mickael Silva

Wonsik Song
Now at NTNU

Ruslan
Khamedov

Suliman
Abdelwahid

Vijayarangan
Vijayamanikandan

Xiao Shao

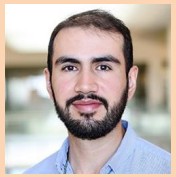

Kevin
Moreno Cabezas

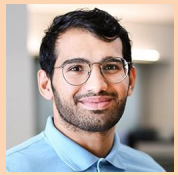

Abdullah Zaihi

Po-Han Chen

Predictive Simulations of Multi-scale Combustion

Direct numerical simulations (DNS) of turbulent flame propagation

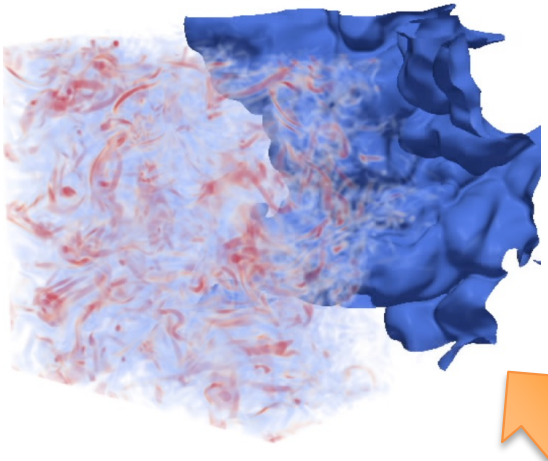

Full-cycle simulations of combustion engines

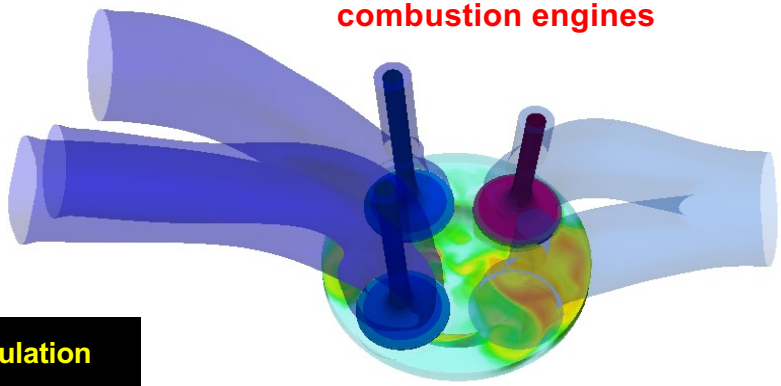

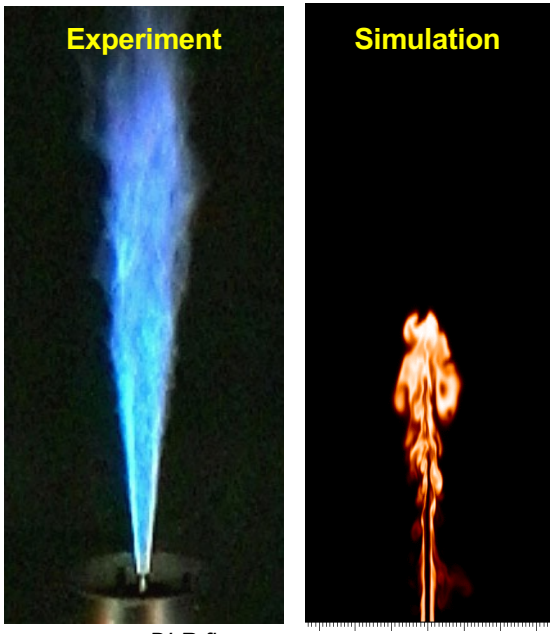

DLR flame

Large eddy simulations (LES) of laboratory-scale flames

High performance computing enables predictive analysis of combustion and pollutant formation, allowing intelligent design of advanced engines at lower development costs.

Towards Green Energy…

Bloomberg
Middle East Edition

Live Now | Markets | Technology | Politics | Wealth | Pursuits | Opinion | Businessweek | Equality | Green

Green
Climate
Politics

EU Lawmakers Remove Last Hurdle to Label Gas, Nuclear as Green

- Parliament votes to approve including gas in taxonomy
- Regulation will most likely enter into force at start of 2023

By John Ainger
July 6, 2022 at 1:21 PM GMT+3 *Updated on July 6, 2022 at 1:56 PM GMT+3*

LIVE ON BLO
Watch Live T
Listen to Liv

Listen to this article
▶ 3:06

Share this article

Follow the authors
@johnainger
+ Get alerts for John Ainger

In this article

European Union lawmakers voted to allow natural gas and nuclear energy to be labeled as green investments, removing the last major barrier to potentially billions of euros of funding from environmental investors.

Parliament fell short of the 353 votes needed to reject the inclusion of gas and nuclear technology in the EU's so-called Taxonomy, a list of economic activities deemed in line with the bloc's transition to climate neutrality. Barring an unlikely objection from member states, it now means the regulation will start at the beginning of next year.

Fit for 55: how the EU will turn climate goals into law

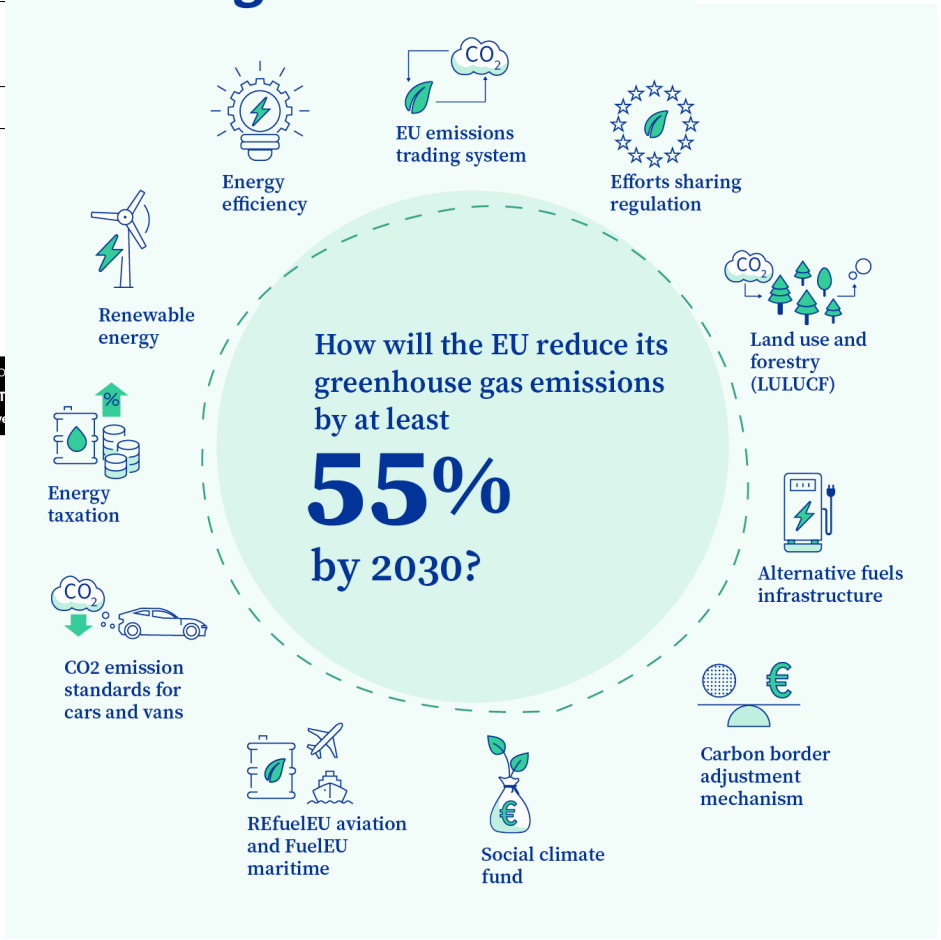

Circular Carbon Economy (CCE)

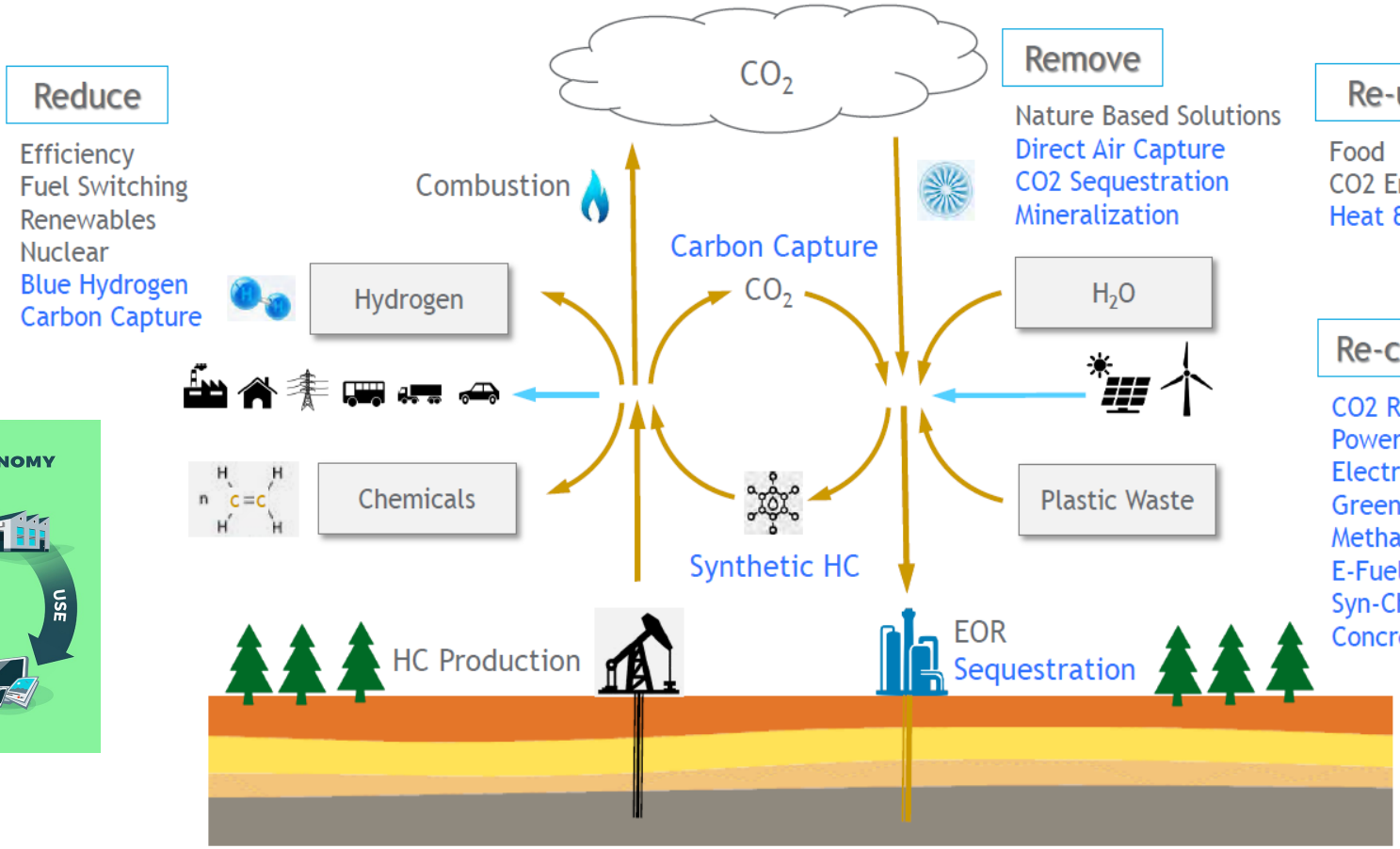

Source: Ahmad Al-Khowaiter, Aramco, IEF-IRENA Seminar, Riyadh, Feb 2020
https://www.ief.org/_resources/files/events/1st-ief-irena-seminar-on-renewable-and-clean-energy-technology-outlooks/ahmad-al-khowaiter.pdf

Power-to-X Is a Viable Solution

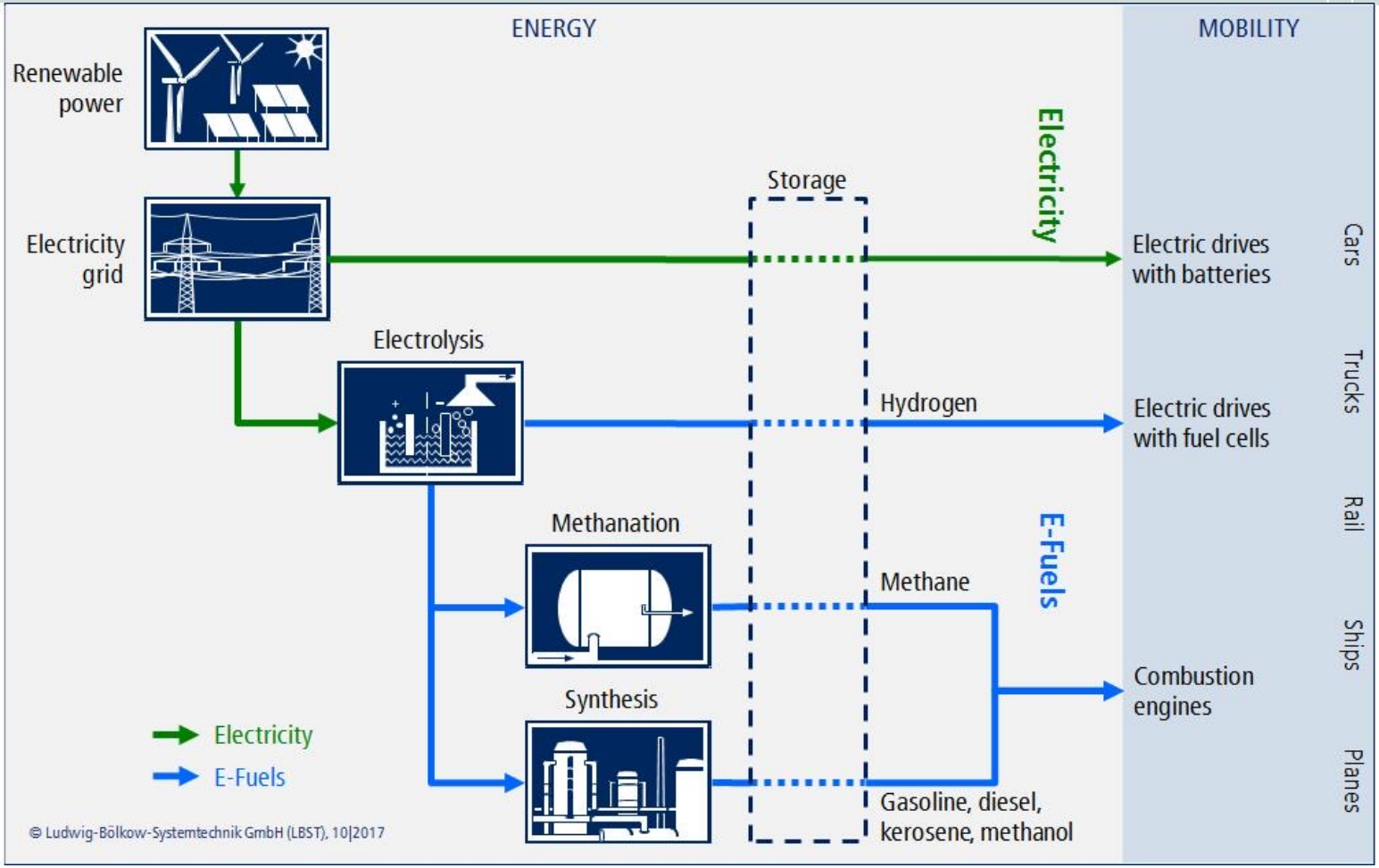

Stefan Siegemund, dena, “The potential of electricity-based fuels for low-emission transport in the EU” (2017)[6]

CCRC Research Forecast

- Drive to decarbonize economy will accelerate
- Cost of energy production from renewables is no longer the barrier
- Combustion will remain a relevant science and technology

Focus research efforts on:

- Sectors that are difficult to decarbonize
  - Heavy duty trucks, marine, aviation, off-grid
  - Cement, mining, smelting
- Energy storage, transportation, utilization
- Employ AI & ML, more diagnostics, better mechanisms, *etc.* to further fundamental understanding of combustion phenomena

CCRC's New Research Areas

- e-Fuels (hydrogen, ammonia, formic acid, methanol, etc.)
- Marine transportation
- Cryogenic carbon capture (CCC)
- Concentrated solar power (CSP) and integration of renewables
- Fuel cells, hydrogen production

Turbulent Hydrogen/Ammonia Premixed Flames at Atmospheric and Elevated Pressure

Contributions by
Francisco Hernandez Perez
Wonsik Song
Ruslan Khamedov

Introduction and motivation

- Hydrogen (H_2) and ammonia (NH_3) have attracted research interests in recent years as viable e-fuels towards carbon-neutral power and transportation

- Despite the simplicity in oxidation pathways, combustion of these fuels involves pronounced effects of fast-diffusing major and intermediate species, leading to interesting flame dynamics in turbulent and high pressure conditions

- Key science/engineering questions:
  - ✓ Flame stability (ammonia)
  - ✓ Flashback (hydrogen)
  - ✓ Differential diffusion effects
  - ✓ NOx

Numerical methods and solver

KARFS (KAUST Adaptive Reacting Flow Solver)

- Fully compressible Navier-Stokes, energy, and species equations
- 8^{th} order central difference scheme for spatial discretization
- 4^{th} order explicit Runge-Kutta method for time integration
- 10^{th} order filter
- Nonreflecting NSCBC (Navier-stokes Characteristic Boundary Conditions)
- Homogeneous isotropic turbulent field by the energy spectrum
- Turbulent forcing
  - Energy spectrum function

  (Passot and Pouquet (1987) J. Fluid Mech.)

$$E(k) = \frac{u'^2}{k_0}\sqrt{\frac{2}{\pi}} \times \left(\frac{k}{k_0}\right)^4 \times \exp\left(\frac{-2k^2}{k_0^2}\right)$$

  - Turbulent forcing scheme

  (Bassenne et al. (2016) Phys. Fluids)

$$A(t) = \frac{\epsilon(t) - G[k(t) - k_\infty]/k_{l,\infty}}{2k(t)}$$

- Reaction mechanism by Burke et al. (9 species and 23 reactions)

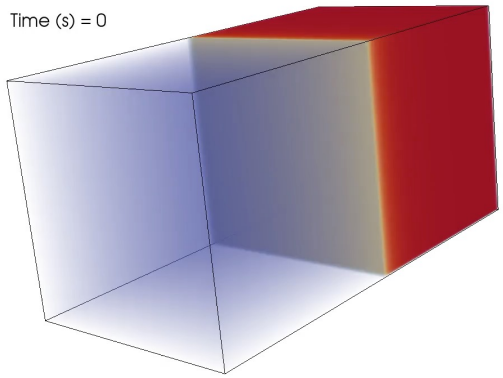

Conditions for various cases

- Borghi diagram

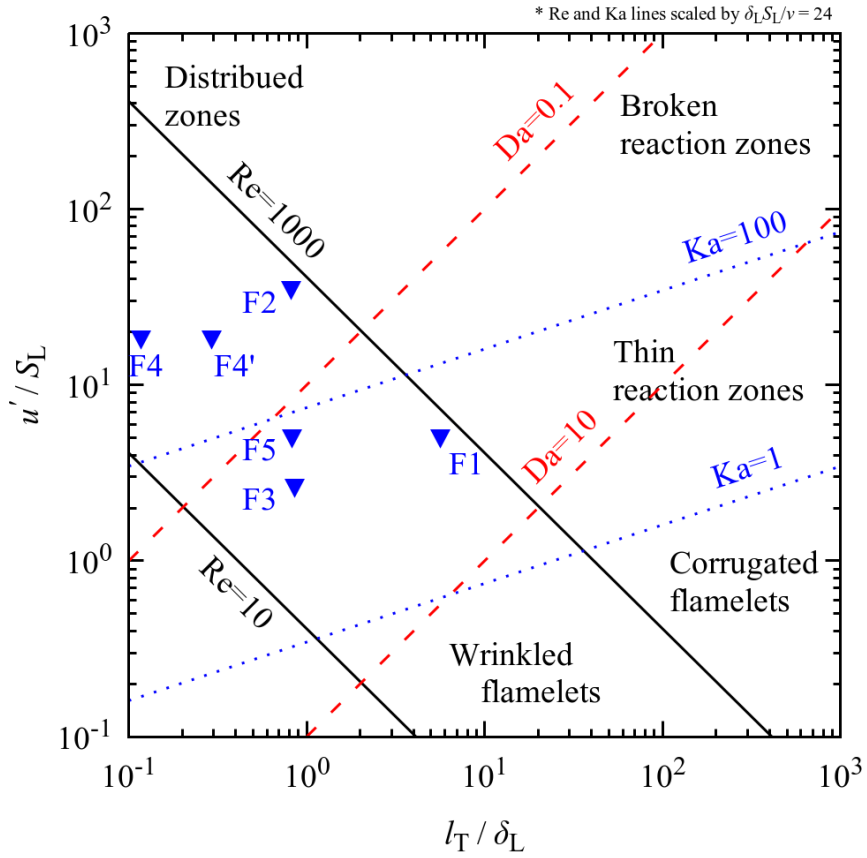

Case	l_T/δ_L [-]	u'/S_L [-]	Re [-]	Da [-]	Ka [-]	$\delta_L/\Delta x$ [-]	Grid [M]	Cost [Mh]
F1	5.65	5	686	1.13	23	17.7	250	6.1
F2	0.82	35	700	0.02	1126	136.2	516	6.3
F3	0.86	2.6	55	0.44	22	17.7	1.3	0.03
F4	0.12	18.3	52	0.01	1126	136.2	15.6	0.39
F5	0.83	5	101	0.17	60	30.8	8.2	0.14
F4′	0.29	18.3	131	0.02	722	131	6.3	0.25

Evolution of temperature and heat release rate (HRR)

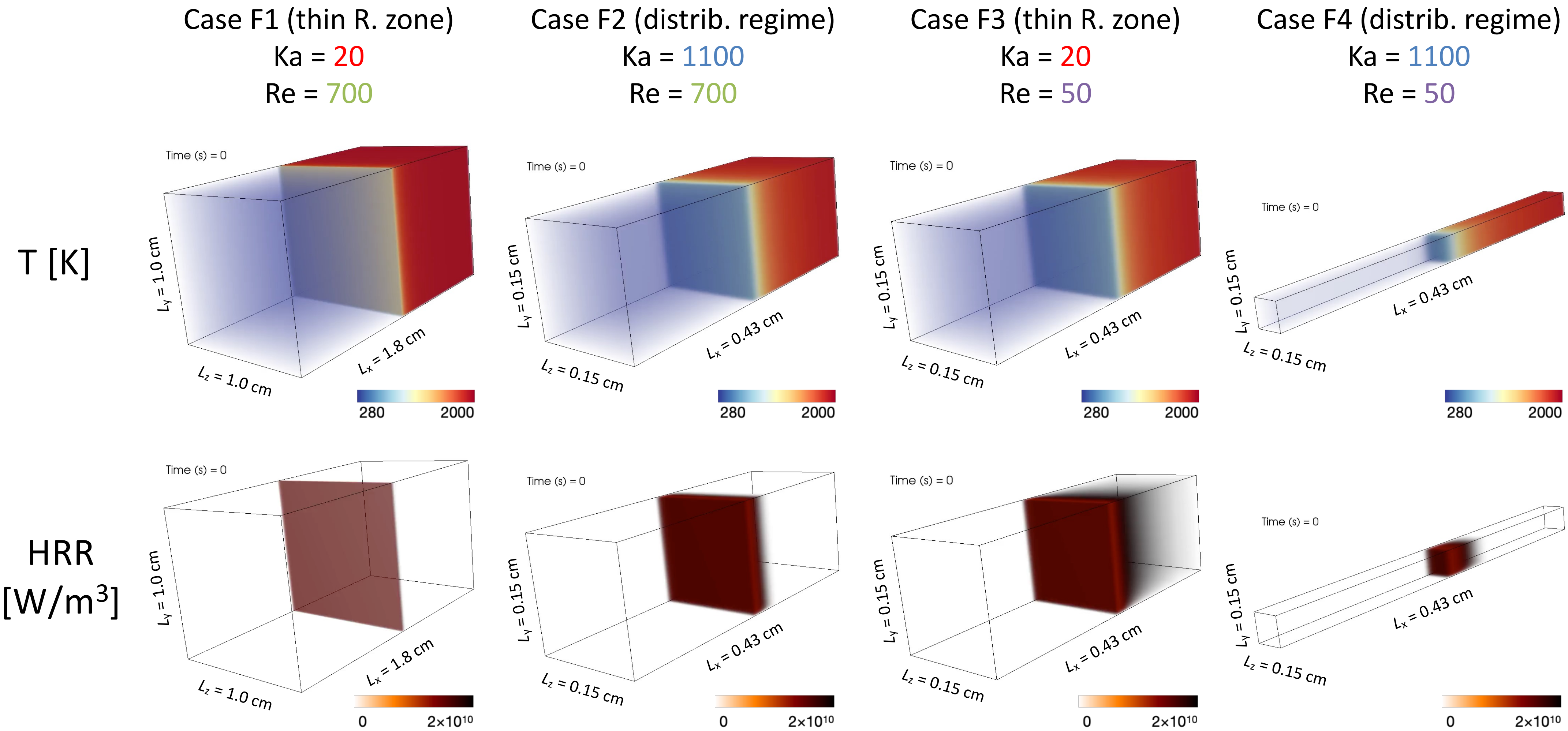

Flame speed definitions

- Turbulent flame speed
  - Fuel consumption speed (global quantity)

$$S_T = \frac{1}{\rho_u (Y_{b,F} - Y_{u,F}) A_0} \int_V \dot{\omega}_F dV$$

Poinsot et al. (1992) CST

  - Density-weighted displacement speed (local quantity)

$$S_d^* = \frac{\rho S_d}{\rho_u} = \frac{1}{\rho \nabla Y_k} [\dot{\omega}_k - \nabla \cdot \mathbf{J}_k]$$

Im and Chen (1999) CNF

Turbulent flame speed and surface area

- Correlation of S_T/S_L vs. A_T/A_L (stretch factor)

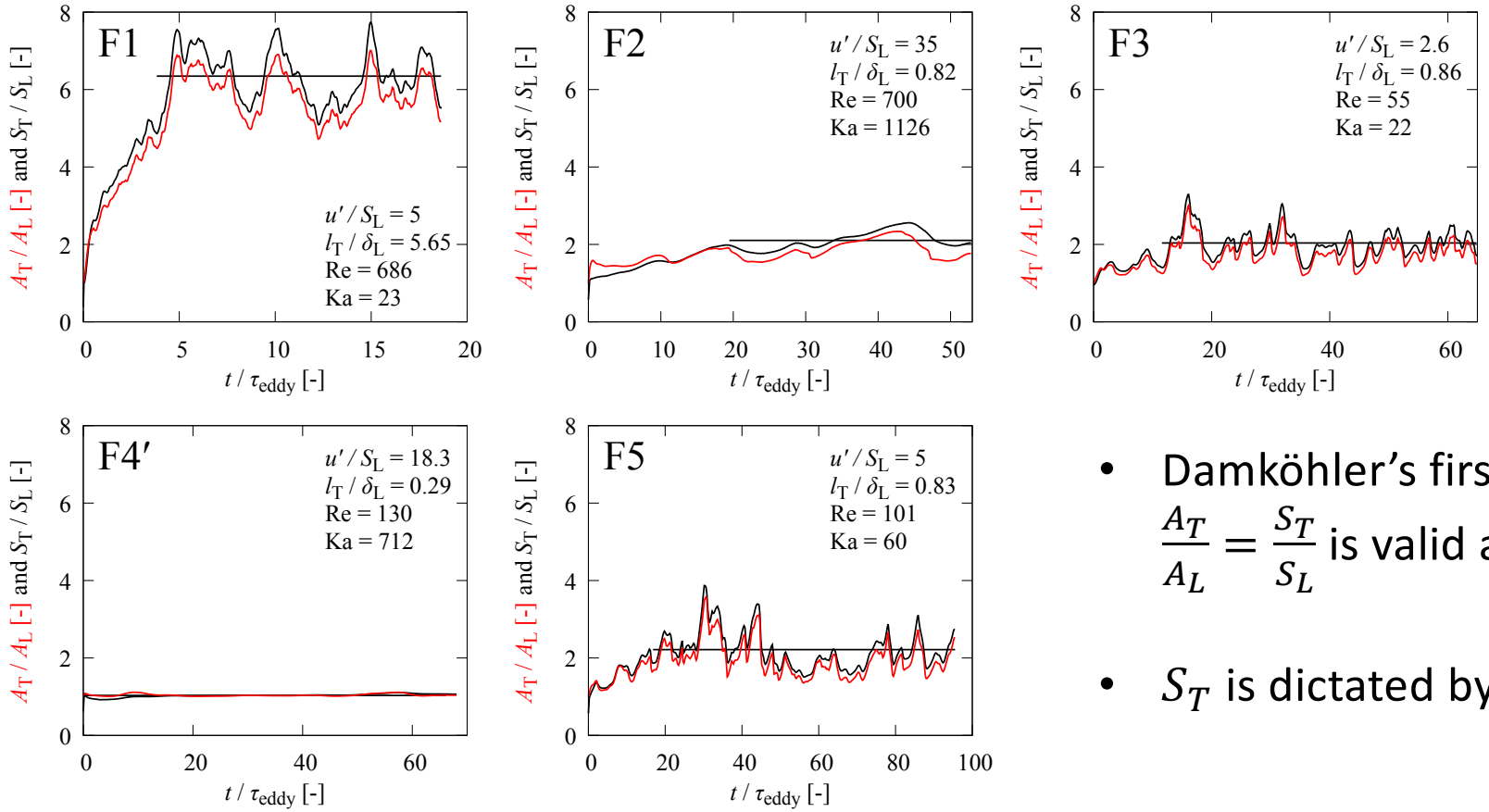

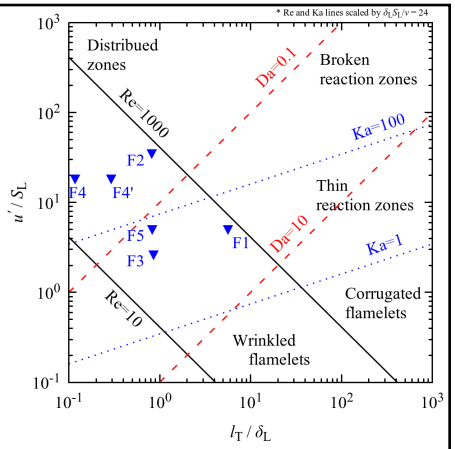

- Damköhler's first hypothesis: $\frac{A_T}{A_L} = \frac{S_T}{S_L}$ is valid at Ka > 1,000
- S_T is dictated by l_T

Integral length scale as key parameter

- Mean stretch factor, mean flame surface area, and mean turbulent flame speed

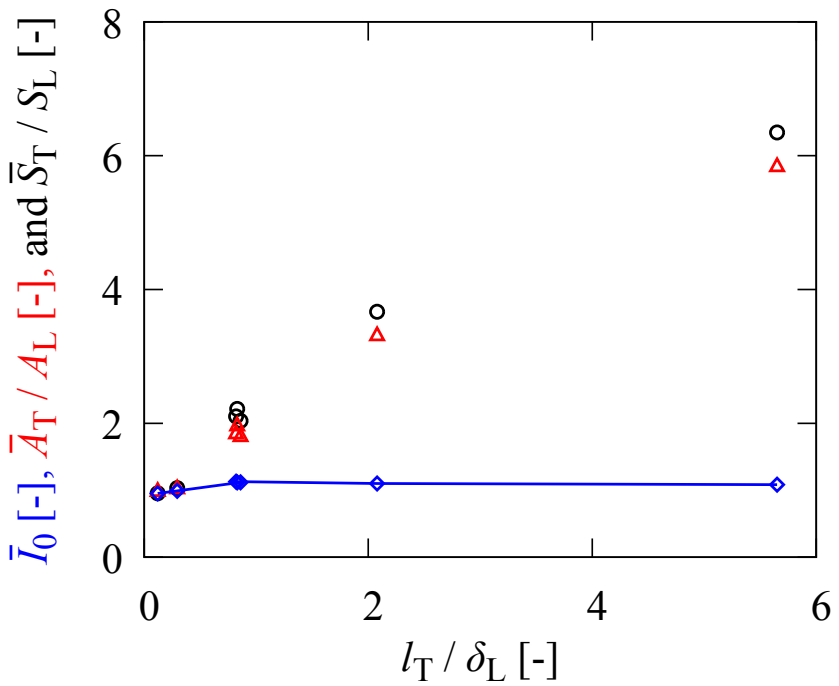

$$\bar{I}_0 = \frac{\bar{S}_T / S_L}{\bar{A}_T / A_L}$$

- For a wide range of l_T and u', $\bar{S}_T$ is correlated well with l_T

Flame structure

$\bar{Y}_i/\bar{Y}_{i,Lmax}$, $\bar{T}/\bar{T}_{Lmax}$: cross-sectional avg. of multiple time steps
Lmax: maximum value at the reference laminar flame

- Cross-sectional averages of temperature and species mass fractions (major)

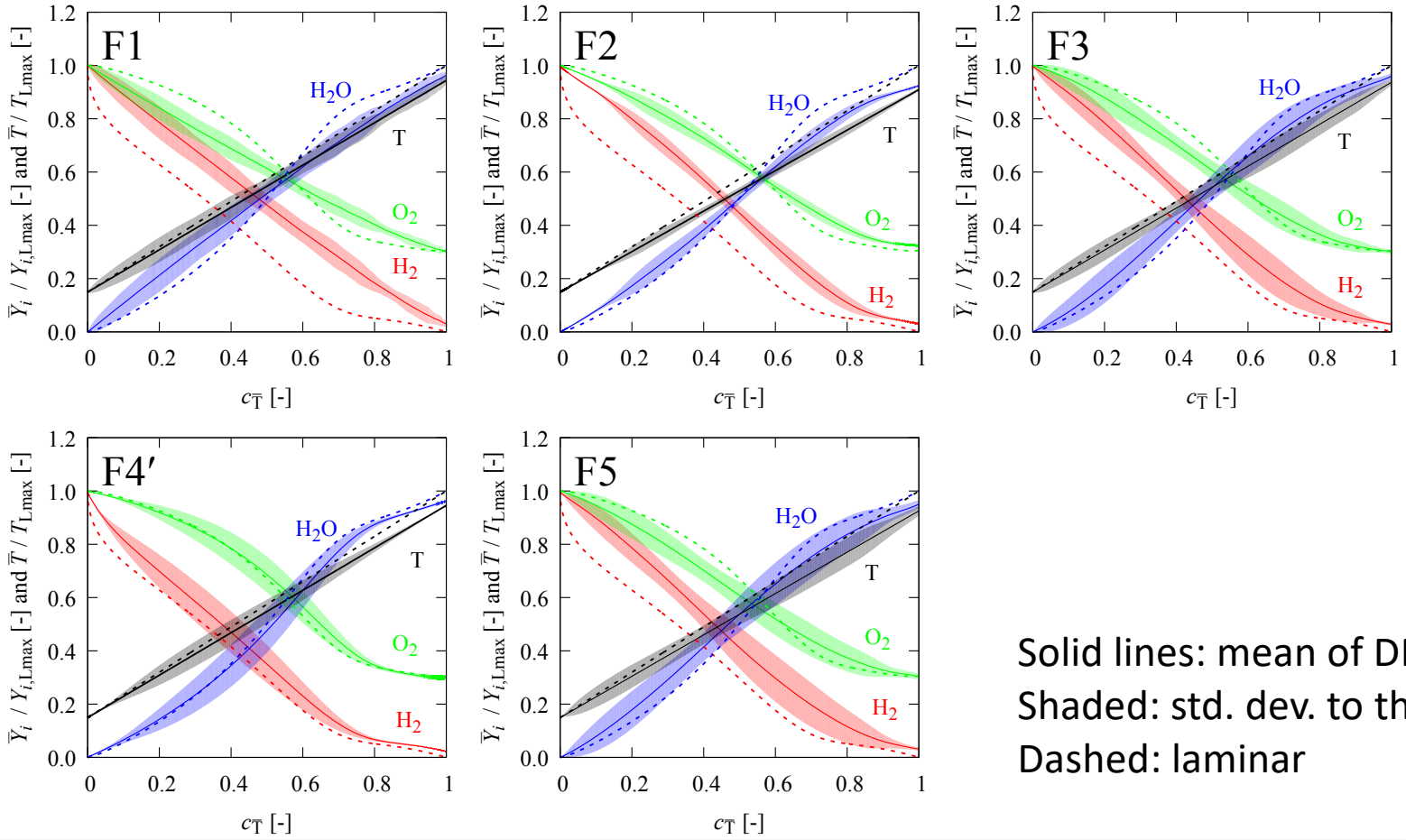

Averaged profiles resemble those of 1D laminar flame

Solid lines: mean of DNS
Shaded: std. dev. to the mean
Dashed: laminar

Conditions to study high pressure effects

- Borghi diagram

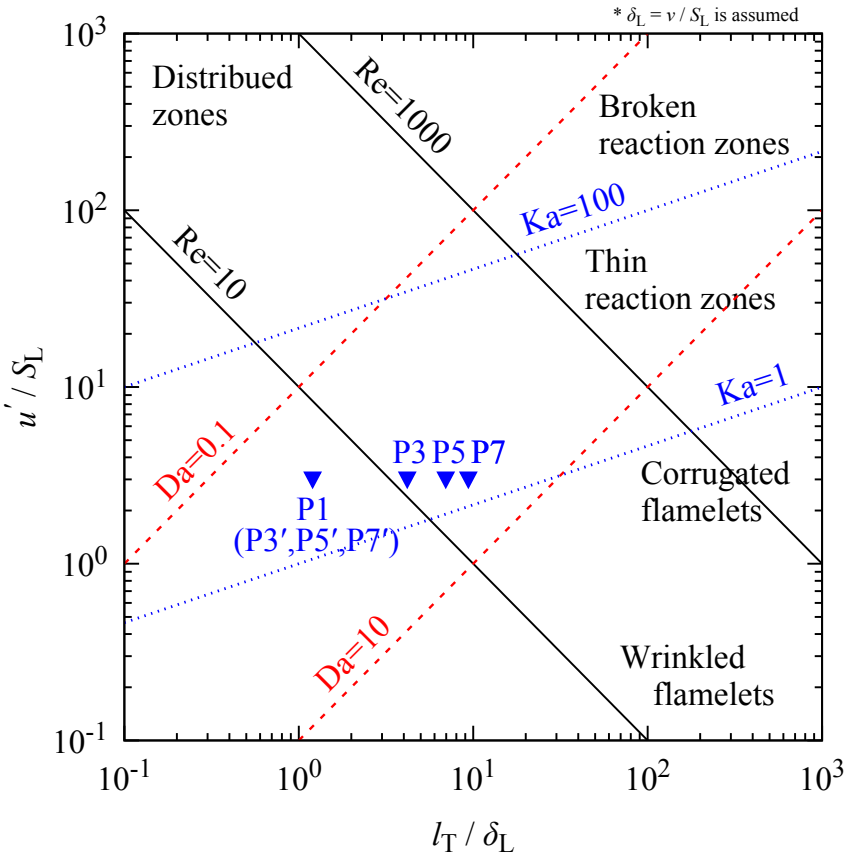

P1 = 1 atm, P3 and P3′: 3 atm, … $\Delta x < \min(2\eta, \delta_L/10)$

Case	l_T/δ_L [-]	u′/S_L [-]	Re [-]	Da [-]	Ka [-]	Δx [μm]	Grid [M]	Cost [Mh]
P1	1.2	3	86.8	0.4	23.3	30.1	1.1	0.005
P3′	1.2	3	58.6	0.4	19.1	10	0.79	0.003
P5′	1.2	3	48.7	0.4	17.4	6	0.79	0.003
P7′	1.2	3	43.3	0.4	16.5	4.56	0.65	0.006

Case	l_T/δ_L [-]	u′/S_L [-]	Re [-]	Da [-]	Ka [-]	Δx [μm]	Grid [M]	Cost [Mh]
P1	1.2	3	86.8	0.4	23.3	30.1	1.1	0.008
P3	4.185	3	204.2	1.395	10.2	10	30.2	0.697
P5	6.958	3	282.4	2.319	7.2	6.13	130.8	2.178
P7	9.374	3	338.6	3.125	5.9	4.56	331.7	7.015

* l_T is identical for P1, P3, P5, and P7

Evolution of temperature and HRR

- For fixed l_T(= 0.428 mm) at a wide range of pressure

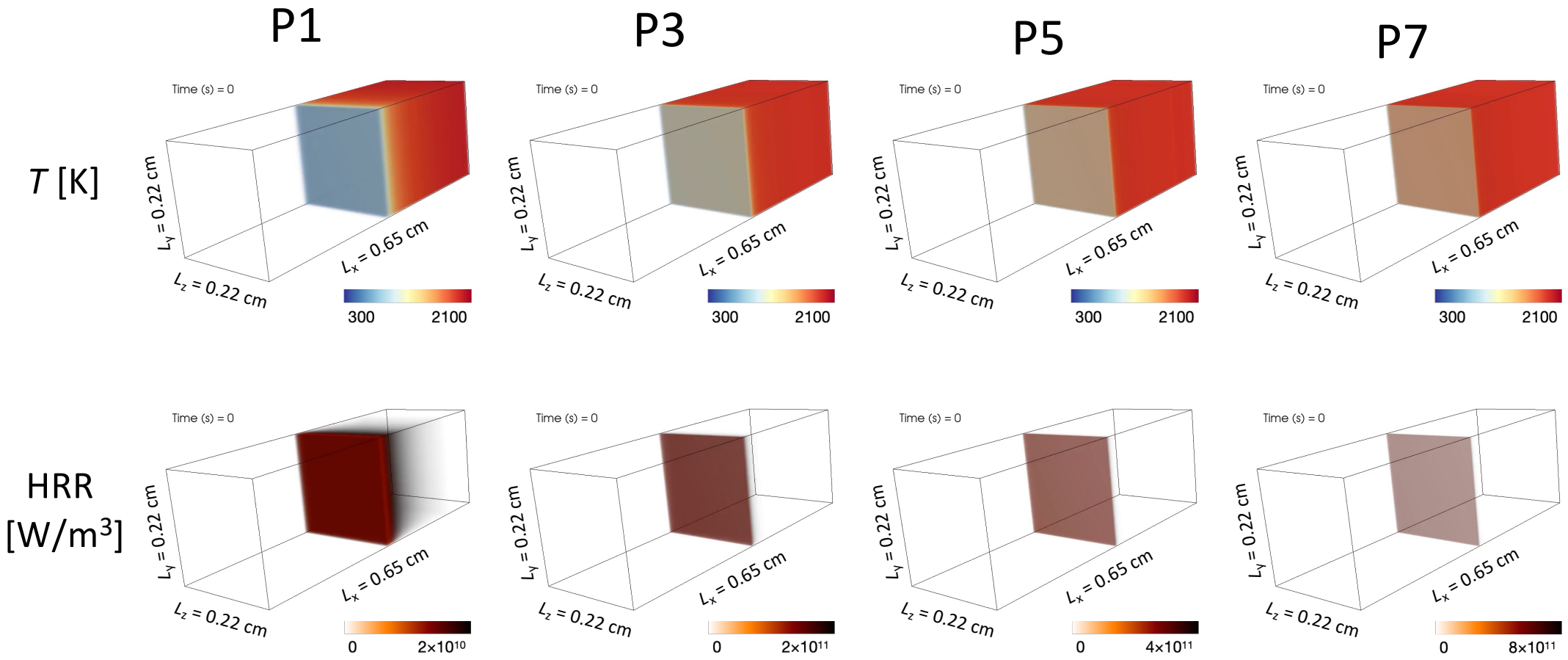

Turbulent flame speed, surface area, and integrated HRR

- Temporal evolution of S_T/S_L, $\omega_{T,V}/\omega_{T,V0}$, and A_T/A_L

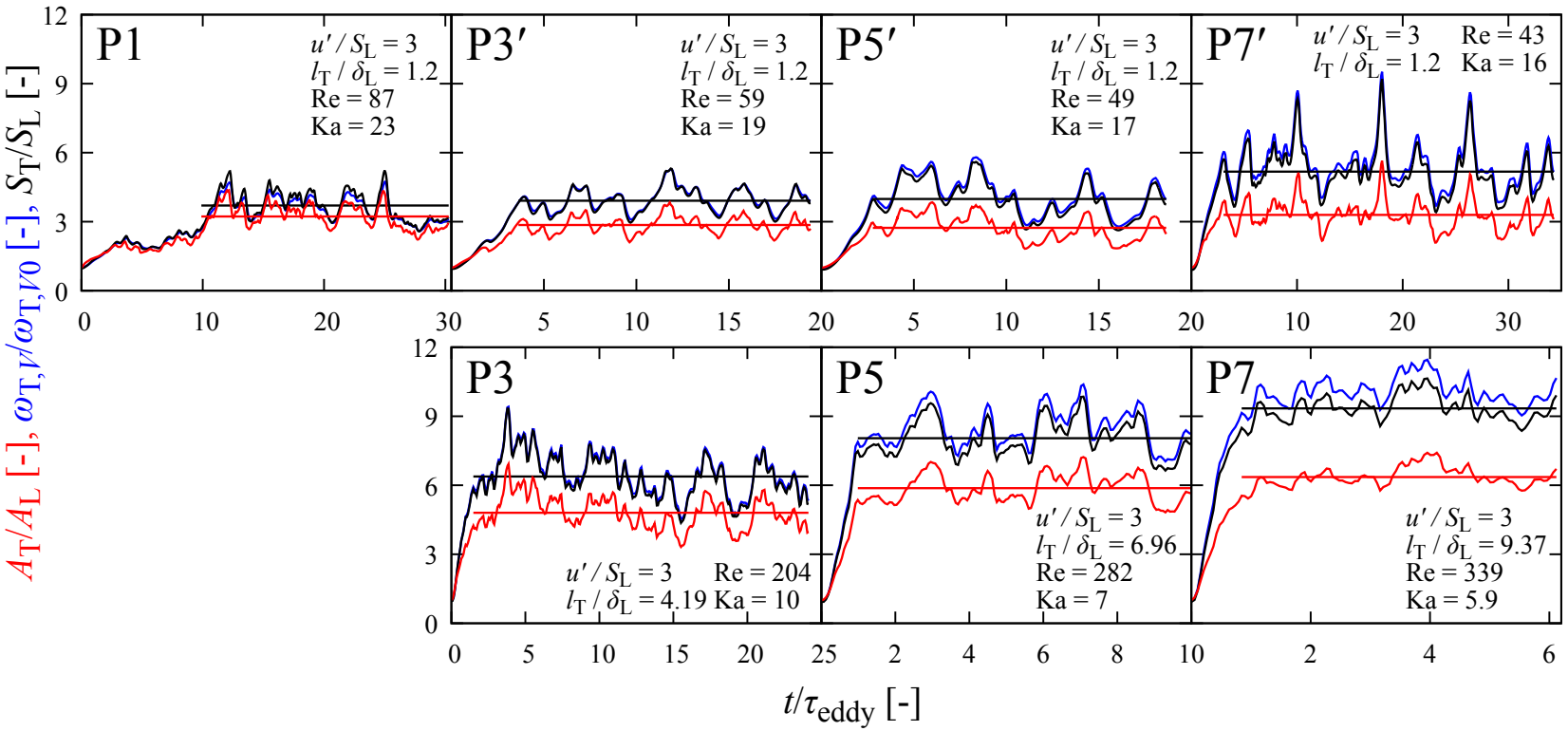

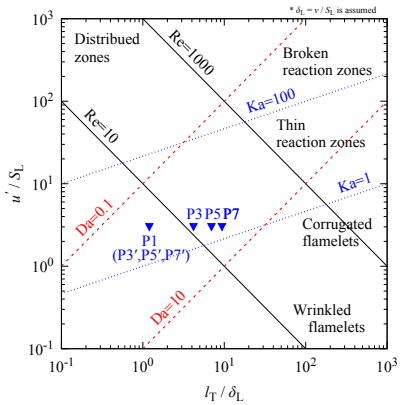

- Chemical effects are pronounced at elevated pressure (reversed trends of S_T/S_L vs. $\omega_{T,V}/\omega_{T,V0}$)
- Volumetric effects (larger HRR for larger domain size)

Displacement speed and curvature distribution

- Probability density functions (PDF) of flame curvature and local displacement speed

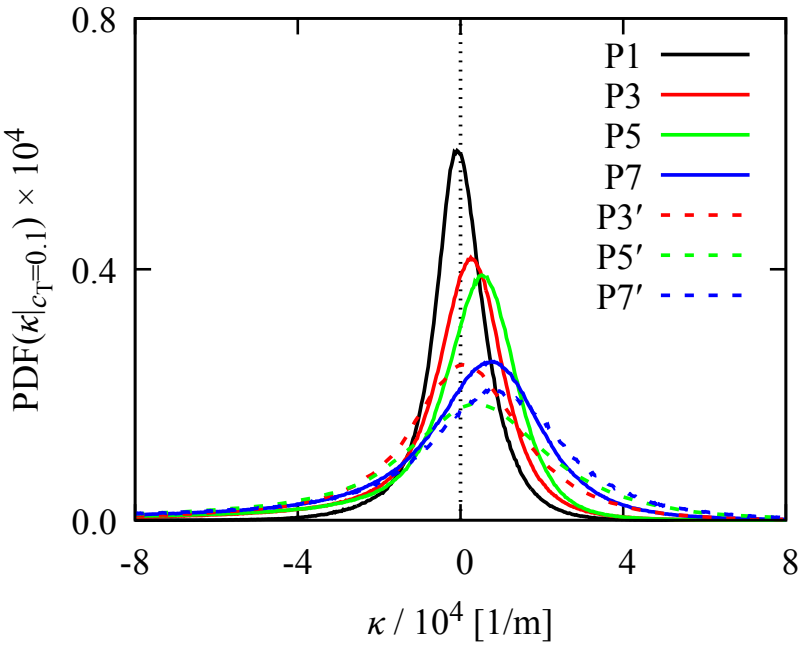

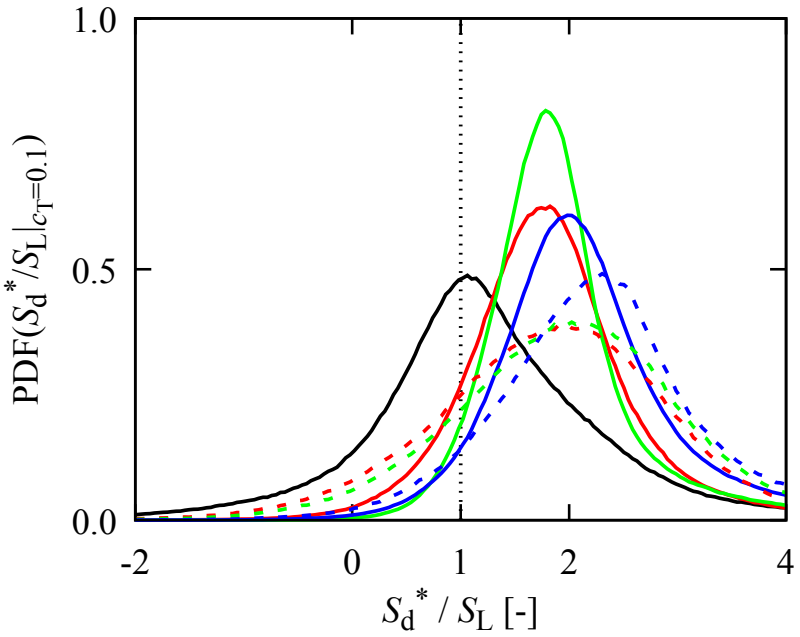

- Clear trend of curvature shifting to positive side as pressure increases
- S_d^* also augments at elevated pressure

Dependence of global quantities on pressure

- Mean stretch factor, mean flame surface area, and mean turbulent flame speed

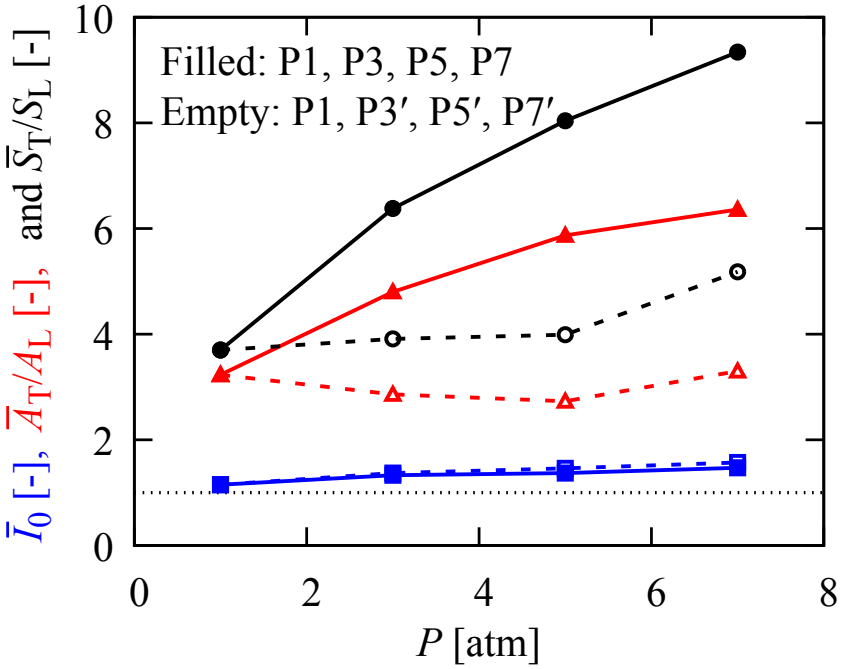

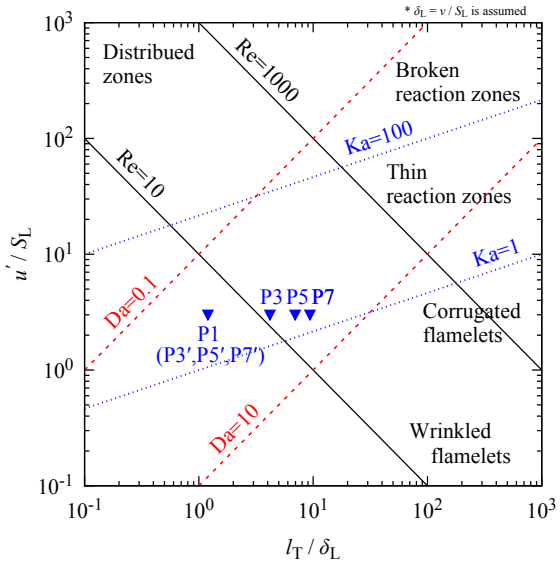

- For the same u'/S_L and l_T/δ_L, S_T/S_L is found to be about the same even at pressure of 5 atm
- Further enhancement of S_T/S_L for P7′

Hydrogen, ammonia lean/rich comparison

- Borghi diagram

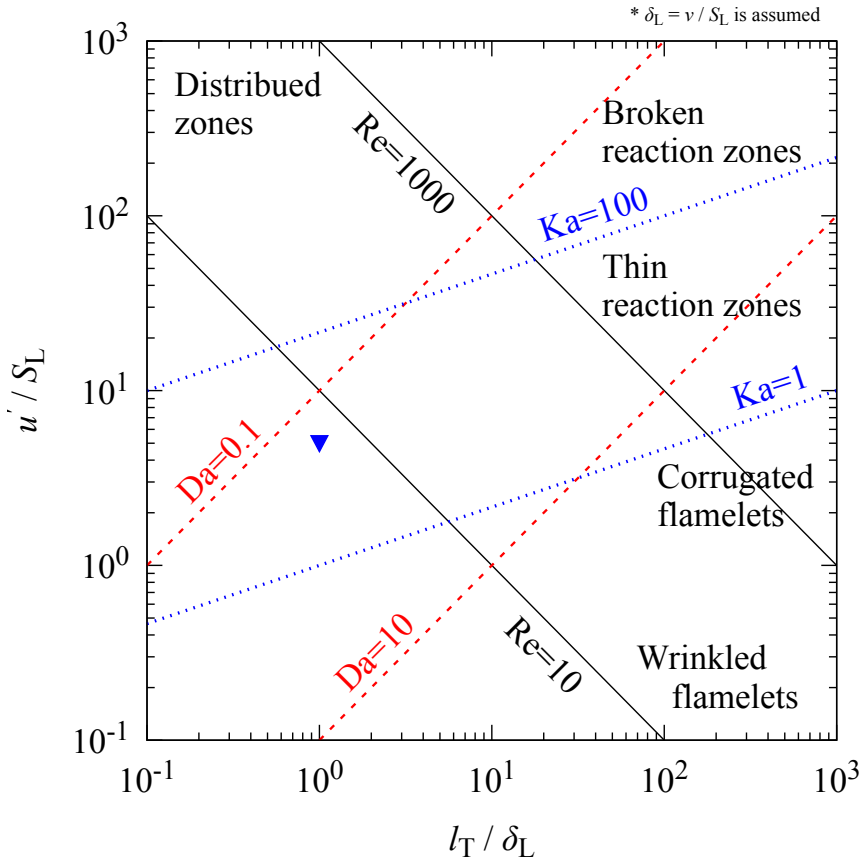

Case	l_T/δ_L [-]	u′/S_L [-]	Re [-]	Da [-]	Ka [-]	$\delta_L/\Delta x$ [-]	Grid [M]
H2	1	10	78	0.1	88	12	0.79
AL	1	10	56	0.1	75	12	0.69
AR	1	10	72	0.1	85	12	1.7

H2: H_2/air premixed flame
φ = 0.41, T = 300 K (S_L = 0.211 m/s), Le = 0.36

AL (lean ammonia): NH_3/air premixed flame
φ = 0.81, T = 600 K (S_L = 0.211 m/s), Le = 0.90

AR (rich ammonia): NH_3/air premixed flame
φ = 1.2, T = 500 K (S_L = 0.211 m/s), Le = 1.12

Unsteady evolution of temperature and HRR fields

H_2/air premixed flame (**H2**)
φ=0.41, T=300 K (S_L=0.211 m/s)
Ka=88, Re=78

NH_3/air premixed flame (**AL**)
φ=0.81, T=600 K (S_L=0.211 m/s)
Ka=75, Re=56

NH_3/air premixed flame (**AR**)
φ=1.2, T=500 K (S_L=0.211 m/s)
Ka=85, Re=72

T [K]

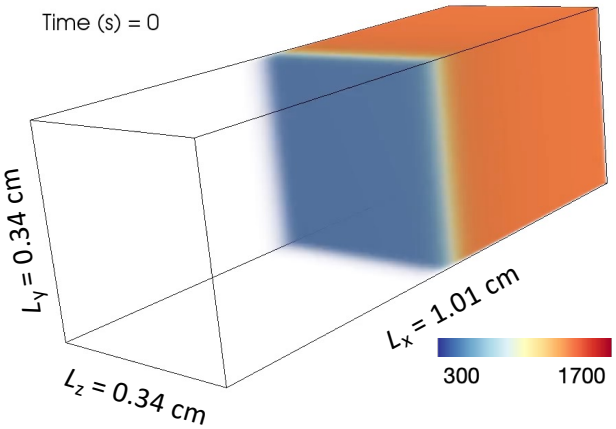

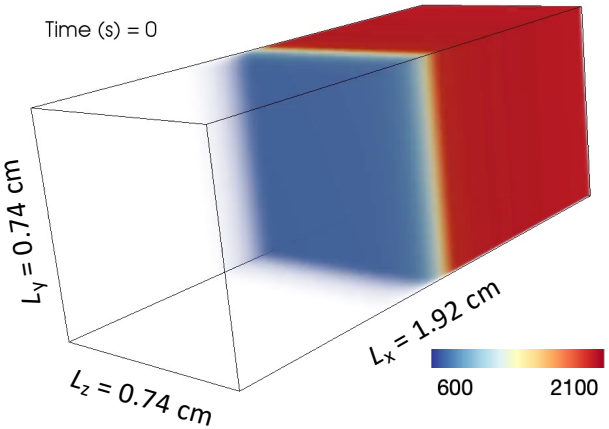

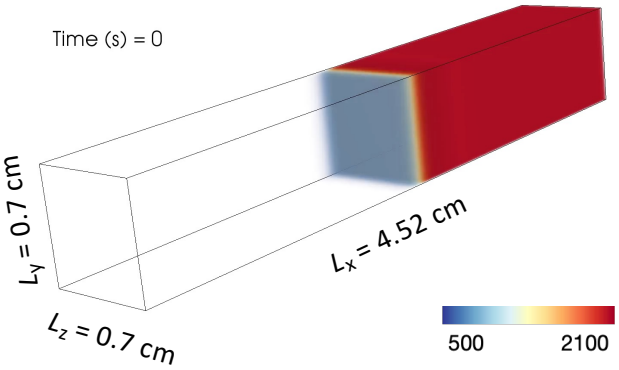

HRR [W/m³]

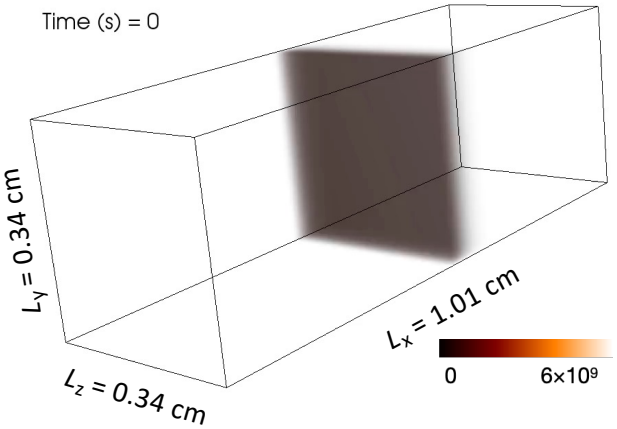

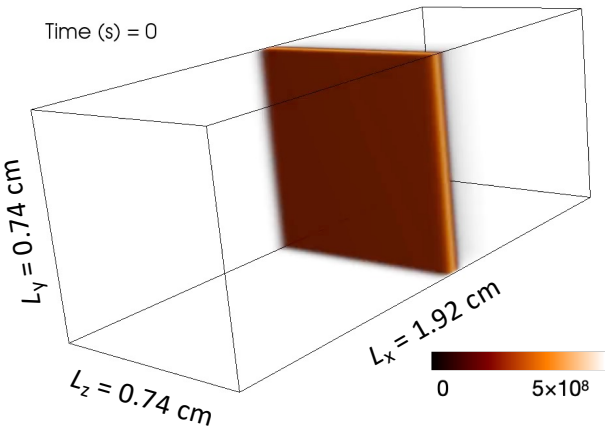

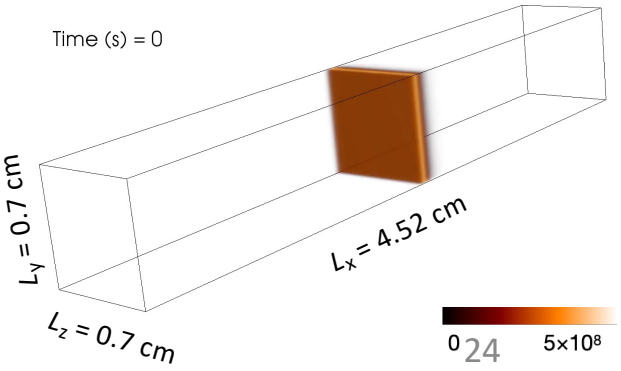

Turbulent flame speed variation

$$S_T = \frac{1}{\rho_u A_0 (Y_{u,F} - Y_{b,F} A_0} \int_V \dot{\omega}_F dV$$

Poinsot et al. (1992) CST

- Temporal evolution of S_T/S_L and A_T/A_L

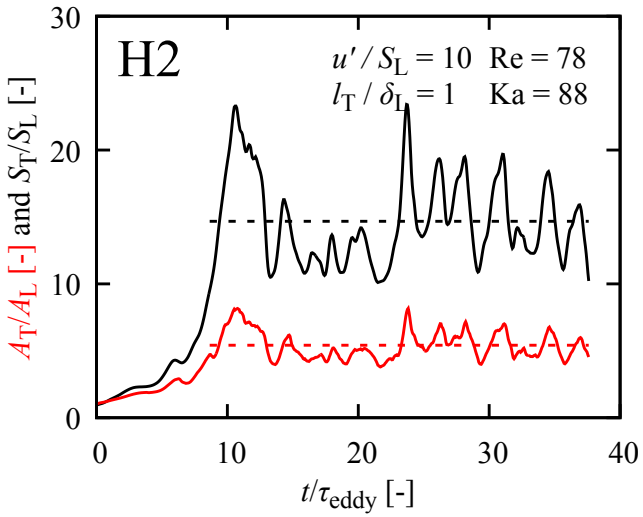

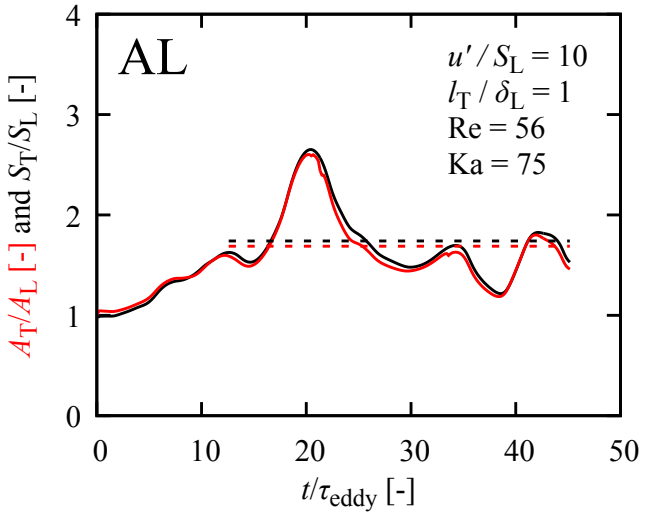

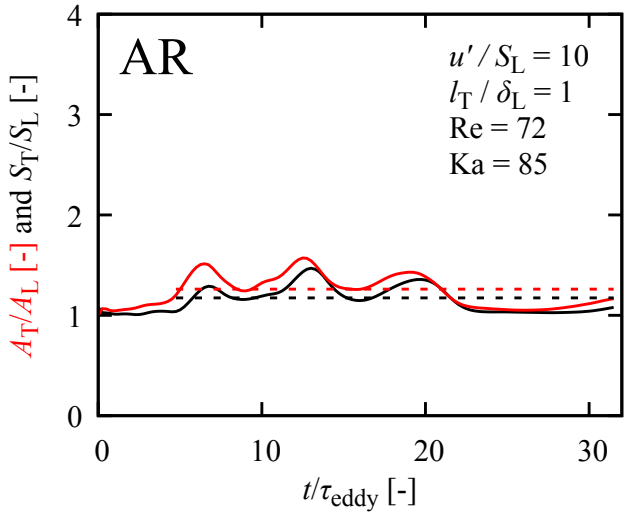

- Large stretch factor for H2 but close to unity for AL and AR
- Despite the same l_T/δ_L and u'/S_L, A_T/A_L and thereby S_T/S_L are very different
- AR has significant reduction of surface area as compared to the lean flame (AL)

Conditional average of heat release rate

- Conditional averages of HRR overlaid with laminar counterpart in progress variable space (c)

c for H2: *T*

c for AL and AR: Y_{H_2O}

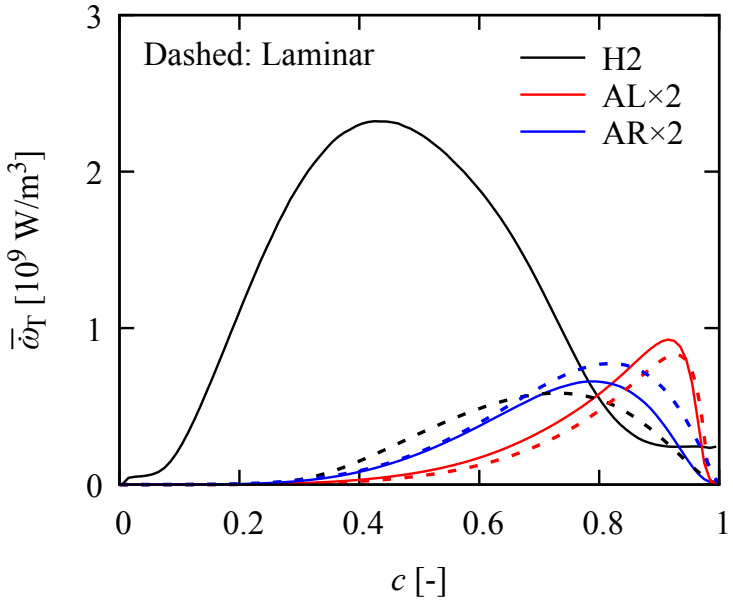

- HRR for turbulent H2 flame:
  1) peak lies more upstream
  2) small bump upstream
  3) larger HRR peak

- HRR for turbulent ammonia flames:
  1) peaks lies more downstream
  2) AL shows higher peak
  3) AR shows broader HRR

Turbulent kinetic energy, temperature and HRR

Cut-off of T: c ≈ 0.01

- Cross-sectional averages of the turbulent kinetic energy, temperature, and HRR

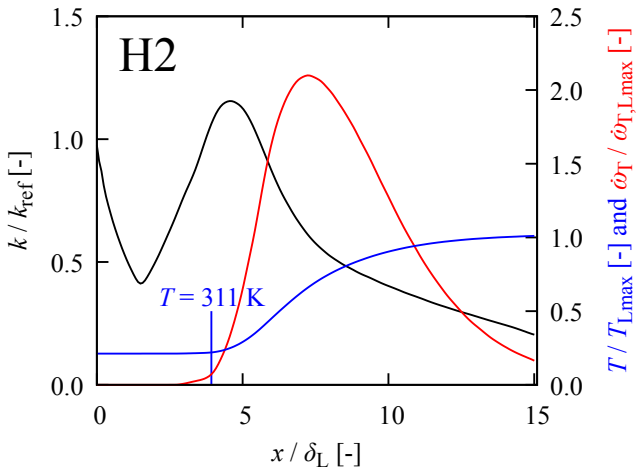

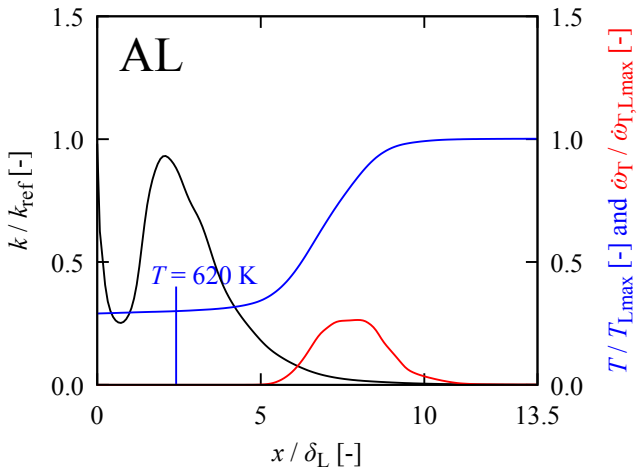

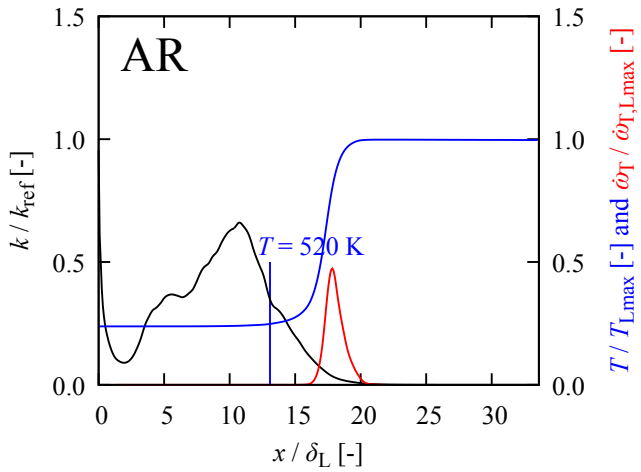

$u_i' = u_i - \bar{u}_i$ where $\bar{u}_i$ is cross-sectional mean for *i*-direction

$k = 0.5 \times (u'^2 + v'^2 + w'^2)$

- Even for the same S_L and u′, TKE for H2 is larger
- Higher degree of thermal-diffusive instability seems to enhance turbulence (TKE)
- Turbulence decays more rapidly for the ammonia flames

Stretch factor of lean and rich ammonia flame

- Mean displacement speed (S_d^*) and stretch $(\mathbb{K})$ along the iso-surfaces of $c_{Y_{H2O}}$

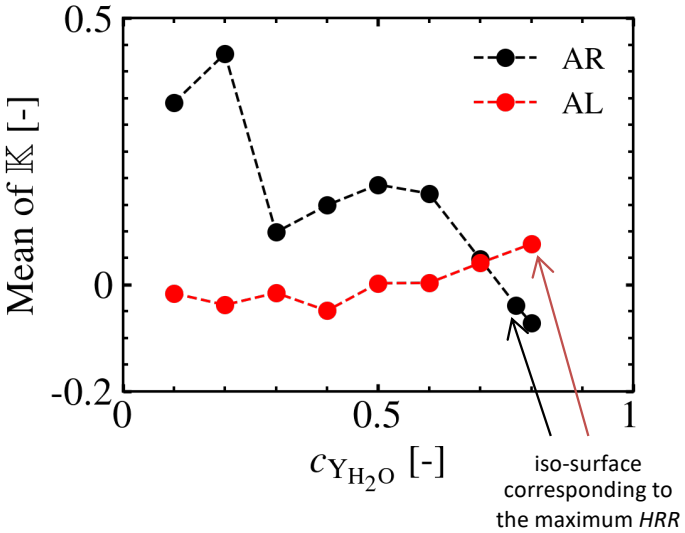

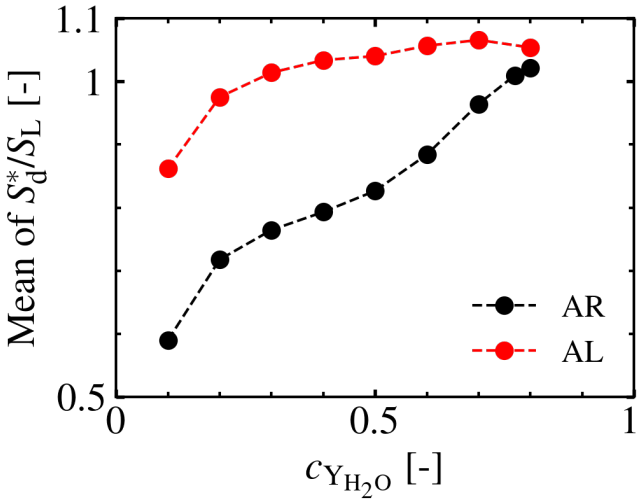

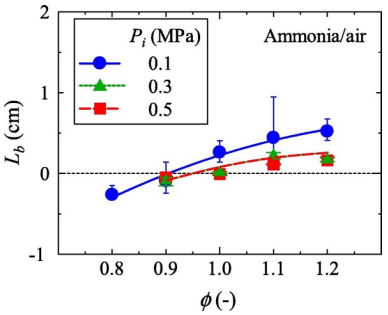

Relationships between burned gas Markstein length, L_b, and equivalence ratio, ϕ
(Hayakawa et.al,2015,Fuel)

- For the rich ammonia flame, the mean stretch is positive in the preheated zone and negative in the intense reaction zone
- The decrease of S_d is a result of stretch, which is responsible for the lower values of $\frac{S_T}{S_L}$ compared to $\frac{\overline{A_T}}{A_L}$ for the rich ammonia flame ---> $\frac{S_T}{S_L} = \frac{\overline{A_T S_d}}{A_L S_L} \approx (1 - \frac{L\bar{\mathbb{K}}}{S_L}) \frac{\overline{A_T}}{A_L}$
- For rich ammonia flame ($Le > 1$), the Markstein number is positive

Effects of turbulence on rich ammonia flames

- Borghi diagram

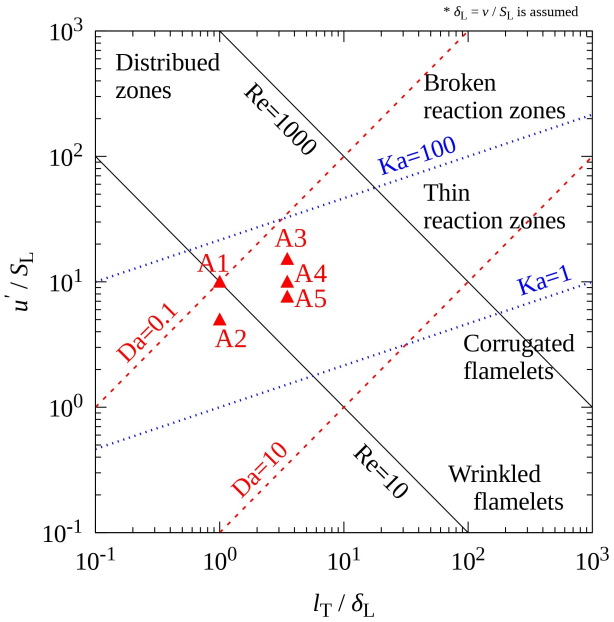

Turbulent cases

- A1 vs. A2: same l_T/δ_L (= 1.0)
- A3 vs. A4 vs. A5: same l_T/δ_L (= 3.5)
- A1 vs. A4: same u'/S_L (= 10)
- A1 vs. A3: same Ka (= 85)
- A2 vs. A5: same Ka (= 30)

- **Only rich ammonia/air flame is considered**: NH_3/air premixed flame φ = 1.2, T = 500 K (S_L = 0.211 m/s)
- The effect of different turbulent conditions is analyzed

Case	l_T/δ_L [-]	u′/S_L [-]	Re [-]	Da [-]	Ka [-]	$\delta_L/\Delta x$ [-]	Grid [M]
A1	1	10	72	0.1	85	12	1.7
A2	1	5	36	0.2	30	12	1.7
A3	3.5	15.2	386	0.2	85	12	16.6
A4	3.5	10	254	0.4	45	11	11.7
A5	3.5	7.6	192	0.5	30	11	11.6

Unsteady evolution of temperature and HRR fields

	A1	A2	A3	A4	A5
l_T/δ_L	1.0	1.0	3.5	3.5	3.5
u'/S_L	10	5	15.2	10	7.6
Ka	85	30	85	45	30

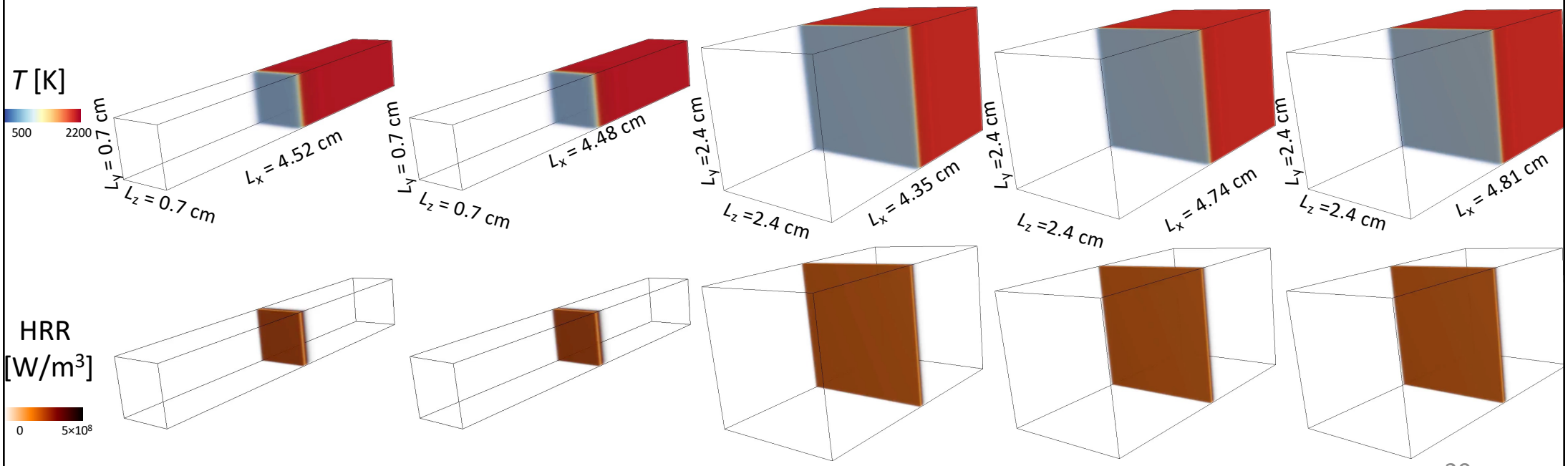

Turbulent flame speed

$$S_T = \frac{1}{\rho_u A_0 (Y_{u,F} - Y_{b,F} A_0} \int_V \dot{\omega}_F dV$$

Poinsot et al. (1992) CST

- Temporal evolution of S_T/S_L and A_T/A_L

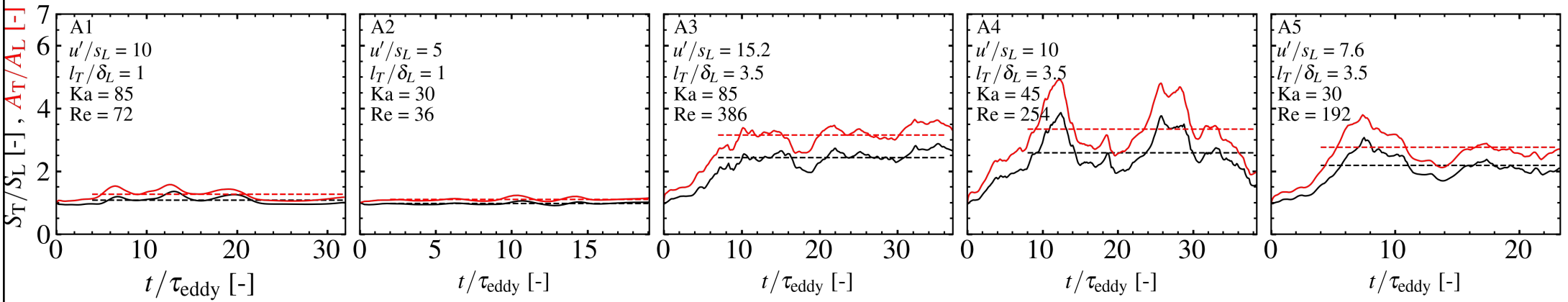

- The mean of the turbulent flame speed is increased with the higher l_T/δ_L
- Less than unity stretch factor is observed regardless of the turbulent conditions
- The stretch factor for high l_T/δ_L flames is decreasing, i.e. the gap between flame area and flame speed enhancement becomes larger

Summary

- The turbulent flame speed displays a strong correlation with l_T/δ_L, the size of the most energetic turbulent eddies.
- Compared to hydrogen flames, turbulence effect is attenuated for ammonia flames due to the different heat release locations.
- The flame stretch factor ($\bar{I}_0 = (\bar{S}_T/S_L)/(\bar{A}_T/A_L)$) changes sign from positive to negative for lean and rich ammonia flames.
- For the rich ammonia flames, the PDF of S_d^* peaks at a value smaller than the one from the 1D laminar flame, and flames have mostly negative curvature.

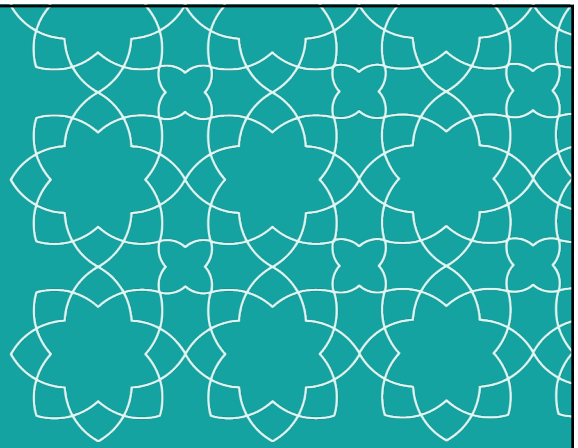

Accelerating Turbulent Reacting Flow Simulations on Many-core/GPUs Using ML and CSP

In collaboration with
University of Rome Sapienza (M. Valorani)
University of Michigan (V. Raman)

KARFS – Performance portable

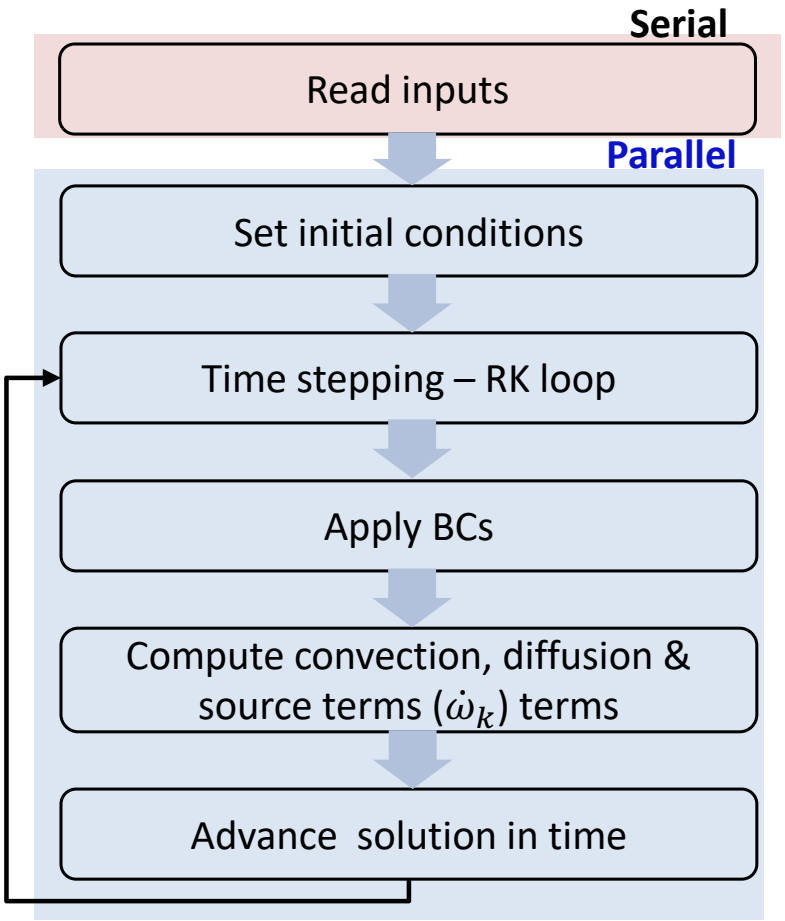

KARFS: KAUST Adaptive Reactive Flow Solver

- Implementation: C++
- Kokkos library: on-node parallelization
- MPI+X (X: Cuda, OpenMP, etc.)
- **Spatial discretization**: WENO7M or CD8
- **Time integration**: RK4 – 6 stages, explicit

Replace

Species source term ($\dot{\omega}_k$): Cantera (CPU-based)

Sequential: per cell computation

with

Species source term ($\dot{\omega}_k$): GPU-based

Matrix-based: wweep over all cells

Impact of GPU chemistry on KARFS DNS solver?

Methodology: matrix multiplication for rates

NC → Number of cells
NS → Number of species
NR → Number of reactions

$$q_j = k_{fj} \prod_k \left(\frac{\rho Y_k}{W_k}\right)^{\nu'_{kj}} - k_{rj} \prod_k \left(\frac{\rho Y_k}{W_k}\right)^{\nu''_{kj}} \in \mathbb{R}^{N_C \times N_S}$$

$$\in \mathbb{R}^{N_C \times N_R}$$

Log space

$$q_j = exp\left(\log \boldsymbol{K}_{fj} + \sum_k \nu'_{kj} \log[X_k]\right) - exp\left(\log \boldsymbol{K}_{fj} - \log \boldsymbol{K}_{cj} + \sum_k \nu''_{kj} \log[X_k]\right)$$

$$\boldsymbol{K}_{fj} = A_j T^{b_j} \exp\left(-\frac{E_{a_j}}{RT}\right)$$

Forward rate constant – Arrhenius form

$$\boldsymbol{K}_{cj} = \frac{p_{ref}^{\sum_k \nu_{kj}}}{RT} \exp\left(\frac{\Delta S_j}{R} - \frac{\Delta H_j}{RT}\right)$$

Equil. rate constant – Polynomials

Linear ANN layer

$$\log(\boldsymbol{K}_{fj}) = \boldsymbol{X}_f \boldsymbol{W}_f + B_f$$

$$\mathbf{x}_f = \begin{bmatrix} \log T_1 & 1/T_1 \\ \log T_2 & 1/T_2 \\ \vdots & \vdots \\ \log T_{N_C} & 1/T_{N_C} \end{bmatrix} \quad \mathbf{W}_f = \begin{bmatrix} \beta_1 & \cdots & \beta_{N_R} \\ -E_1/R & \cdots & -E_{N_R}/R \end{bmatrix} \quad B_f = \begin{bmatrix} \log A_1 \\ \log A_2 \\ \vdots \\ \log A_{N_R} \end{bmatrix}^T$$

Matrices of rate parameters in log space

Performance assessment

Chemistry (source term) only compute time comparison: CPU (Cantera) vs GPU (UMChemGPU)

- **GPU node:** Intel(R) Xeon(R) CPU E5-2699 v3, 230 GB node memory, and 16 GB memory per GPU and one P100 (Pascal) GPU
- **Chemistry**: H2-air (NS=9 & NR=23) Burke et al.
- Min **10X** faster source term for 10^3 grid block size (on GPU)
- Max O~10^3 speedup for 100^3 grid size

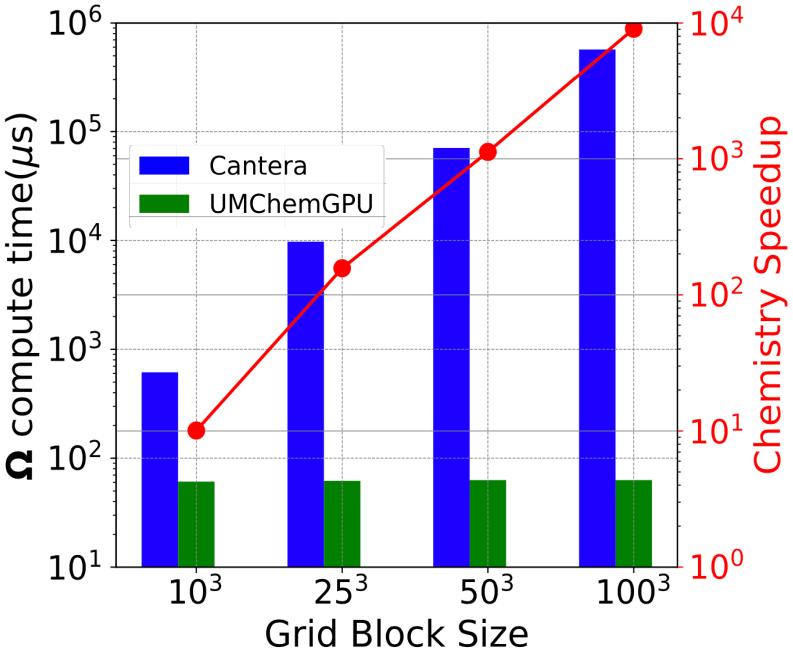

- Significant faster (O~10^3) source term computation with GPU chemistry
- What about overall performance gain??

1. MPI+OpenMP (CPU parallel) DNS code

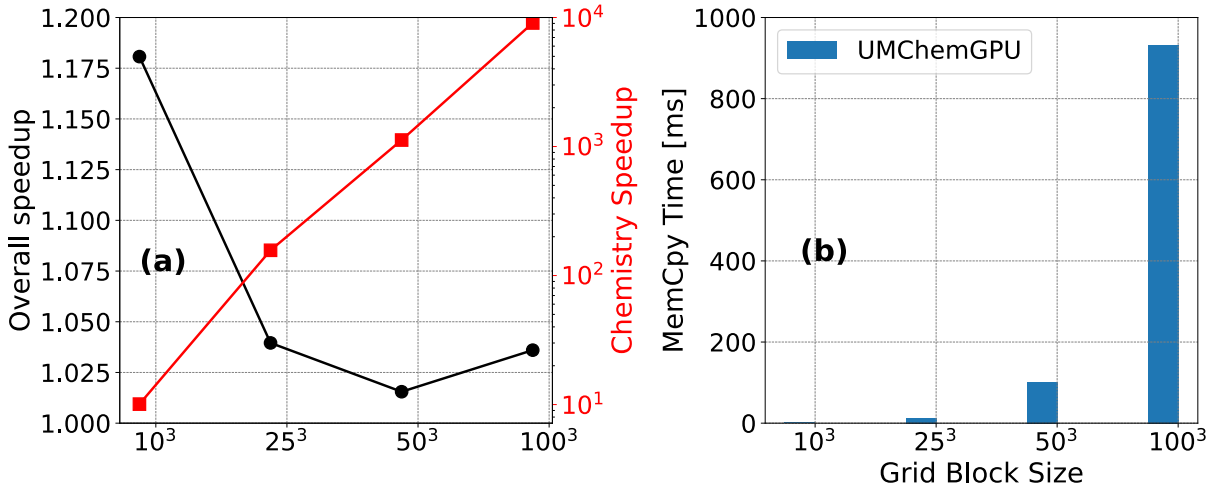

Time overall speedup: Convection+diffusion+time integration+dealiasing filter (except I/O)

- **Chemistry**: H_2-air (NS=9 & NR=23) Burke et al.
- Up to O(**$10^{3)}$** source term Speedup
- Maximum **18%** gain in overall speedup
- **Reason**: data copy time between host-to-device (T, P, ρ, Y_k) and device-to-host ($\boldsymbol{\Omega}$) memory spaces
- **Solution:** compile DNS code for GPUs (MPI+CUDA)

CPU/GPU Memory spaces

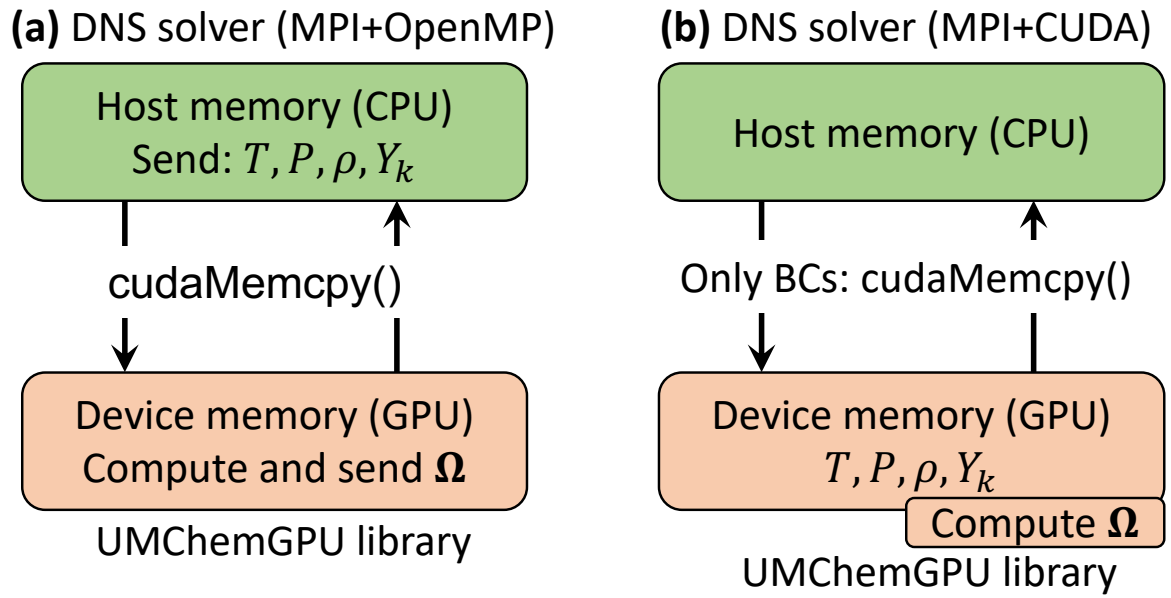

- Memory spaces of CPU and GPU **differ**
- DNS code **MPI+OpenMP**: data copy (host-to-device & device-to-host) required
- DNS code **MPI+Cuda**: data copy (host-to-device & device-to-host) **NOT** required

Data copy across memory spaces is important

2. MPI+CUDA (GPU parallel) DNS code

Chemistry: H_2-air (NS=9 & NR=23) Burke et al

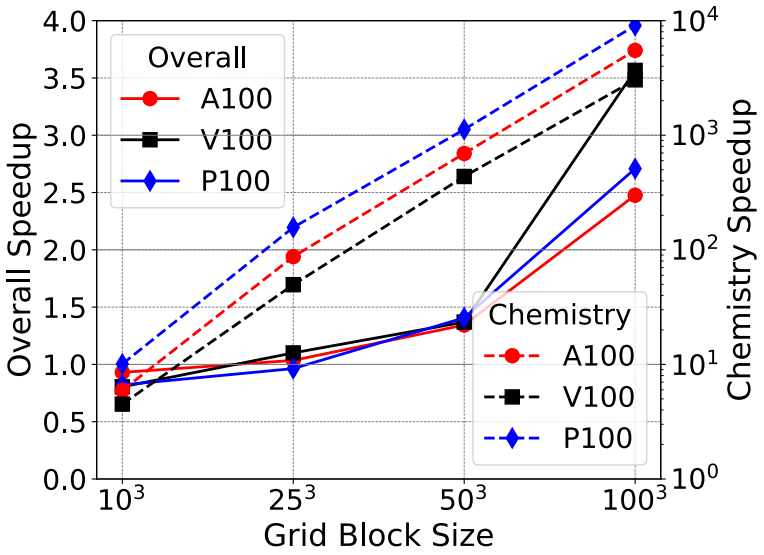

- DNS solver: MPI+CUDA
- Time per step: transport + time integration + dealiasing filer (except I/O)
- 1 MPI + 1 CUDA (Time integration + transport + filter + Chemistry)

DNS solver – MPI+CUDA

Species source term
Cantera – CPU-based

Species source term
UMChemGPU – GPU-based

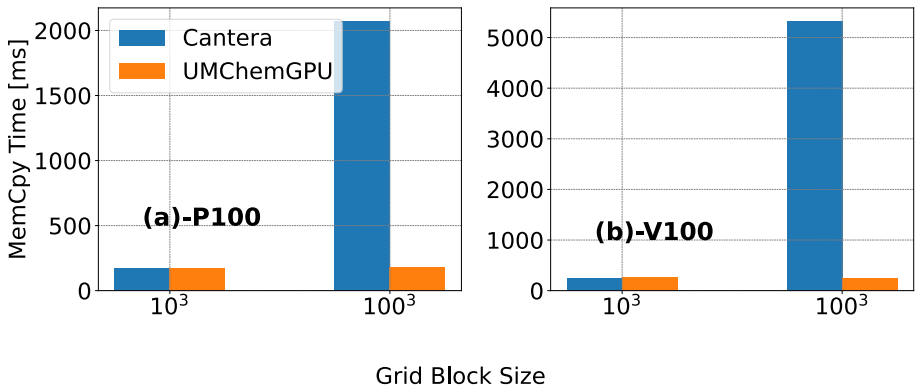

MPI+CUDA+Cantera vs. MPI+CUDA+GPU Chemistry

- 3.5X overall speedup using GPU chemistry (100^3 cells)
- Matrix-based formulation of chemistry & cuBLAS
- Efficient utilization of GPU
- Minimal data copy time

Roofline model: GPU chemistry

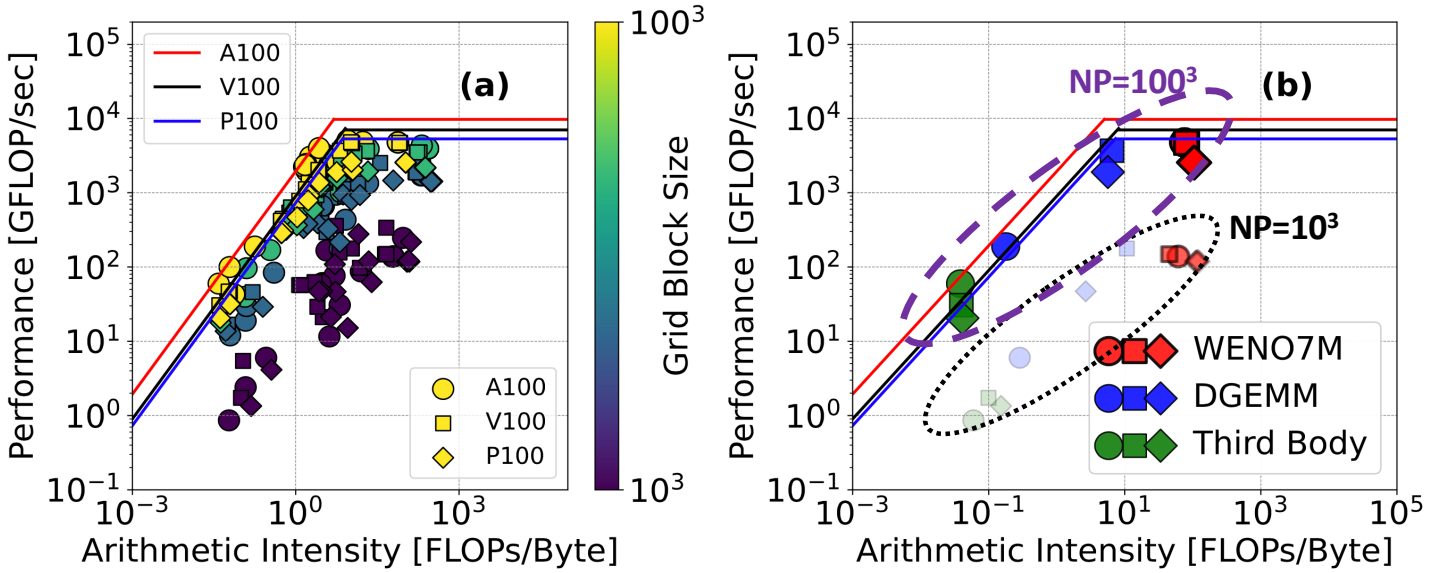

- Poor GPU utilization for **10^3 cells** → Overall **poor** performance
- Effective GPU utilization for **100^3 cells** → **Max performance** gain

DAXPY: $z = a * x + y$
2FLOPs: 1 add, 1 mult.
2 read (x, y) & 1 write (z) = 8*3 = 24 bytes
X-axis: AI = $2/24 = 0.0833$

Computational Singular Perturbation (CSP)

- **CSP** – Automated computational algorithm to decompose characteristic time scales of a dynamical system.

Lam and Goussis, 1989

- For species and energy equations

Original form of the system:

$$\frac{d\boldsymbol{z}}{dt} = \boldsymbol{g}(\boldsymbol{z}), \quad \boldsymbol{z} \in \mathbb{R}^{N+1}$$

z: statevectors (T and Y_i)
g: chemical source term

CSP form of the system:

$$\frac{d\boldsymbol{z}}{dt} = I \cdot \boldsymbol{g} = A\,(B \cdot \boldsymbol{g}) = \sum_{i=1}^{N+1} \boldsymbol{a}_i\, f^i = \sum_{r=1}^{M} \boldsymbol{a}_r\, f^r + \sum_{s=M+1}^{N+1} \boldsymbol{a}_s\, f^s.$$

Mode timescales: $\tau_1 < \cdots < \tau_M \ll \tau_{M+1} < \ldots < \tau_N$

Fast subspace **Slow subspace**

$$\tau_i = \frac{1}{|\lambda_i|}$$

$$\frac{d\boldsymbol{z}}{dt} \approx \sum_{s=M+1}^{N+1} \boldsymbol{a}_s\, f^s = \left(\sum_{s=M+1}^{N+1} \boldsymbol{a}_s\, \boldsymbol{b}^s \right) \boldsymbol{g} = P\,\boldsymbol{g}$$

$$f^r \approx 0 \qquad r = 1, \ldots, M$$

$$\boldsymbol{z}(t_{n+1}) = \boldsymbol{z}^* - \sum_{r=1}^{M(\boldsymbol{z}^{\mathcal{M}})} \boldsymbol{a}_r(\hat{\boldsymbol{z}})\, f^r(\hat{\boldsymbol{z}}, \boldsymbol{z}^*)\, \tau^r(\hat{\boldsymbol{z}})$$

Radical correction

$$f^i = \boldsymbol{b}^i \cdot \boldsymbol{g},$$

$$\mathbf{b}^i \cdot \mathbf{a}_j = \delta^i_j$$

$\mathbf{a}_n$: CSP column basis vector of the n-th mode (approx. right eigenvector of the Jacobian of **g**)

$\mathbf{b}^n$: CSP row basis vector of the n-th mode (approx. left eigenvector of the Jacobian of **g**)

f^n: amplitude of the n-th mode

δ^i_j: Kronecker delta

CSP solver algorithm

1) Compute CSP basis

$$J(\mathbf{g}(\mathbf{y}))\mathbf{a}_k = \lambda_k \mathbf{a}_k$$ (eigensystem of the Jacobian)

2) "radical" correction to apply fast scales (and get back onto manifold)

$$\boldsymbol{y}^{\mathcal{M}}(t) = \boldsymbol{y}(t) - \sum_{r=1}^{M} \boldsymbol{a}_r f^r \tau^r$$

3) Compute # of exhausted modes (M)

$$\vec{g} = \overbrace{\sum_{k=1,2,\ldots,M} f^k \vec{\mathbf{a}}_k}^{\text{'small'}} + \sum_{k=M+1,M+2,\ldots,N} f^k \vec{\mathbf{a}}_k$$

4) Build CSP Projection Matrix

$$P(t) = I - \sum_{r=1}^{M} \boldsymbol{a}_r \boldsymbol{b}^r$$

5) explicit integration of slow modes

$$\frac{d\mathbf{y}}{dt} = \sum_{s=M+1}^{N} \mathbf{a}_s f^s = P \cdot \vec{g}(\mathbf{y}^{\mathcal{M}})$$

$$\frac{dT}{dt} = -\sum_{i=1}^{N} \frac{h_i}{c_p} P \cdot \vec{g}(\mathbf{y}^{\mathcal{M}}) = -\sum_{i=1}^{N} \frac{h_i}{c_p} \vec{g}_{slow}(\mathbf{y}^{\mathcal{M}})$$

6) "radical" correction to apply fast scales (and get back onto manifold)

$$\boldsymbol{y}(t+\delta t) = \boldsymbol{y}^*(t) - \sum_{r=1}^{M} \boldsymbol{a}_r f^r \tau^r$$

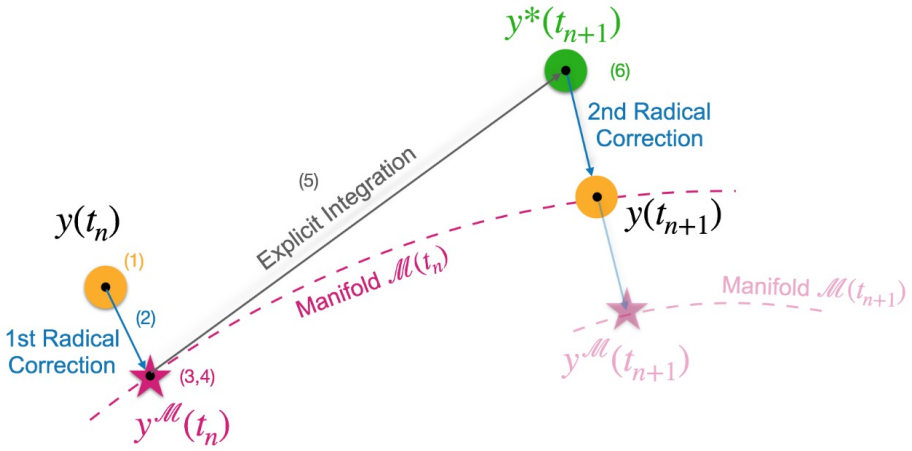

CSP solver algorithm

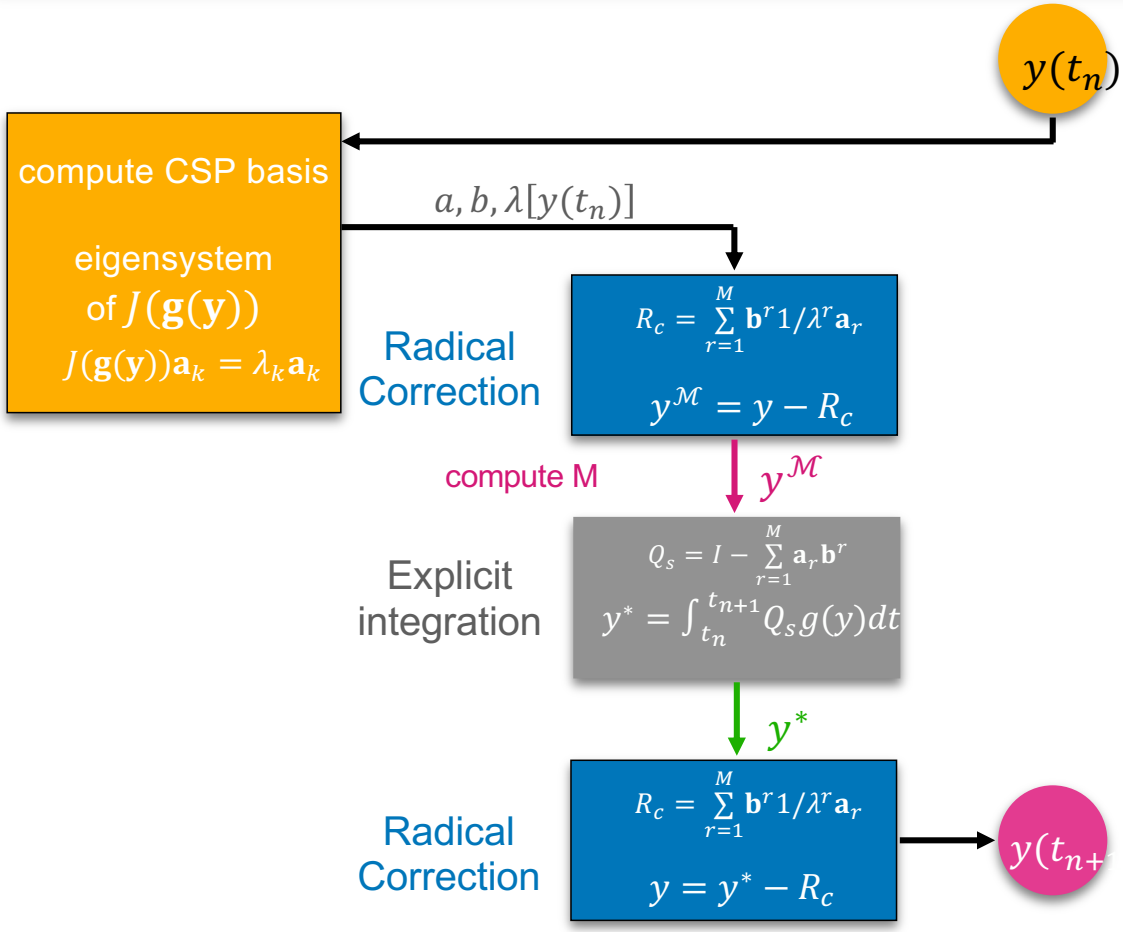

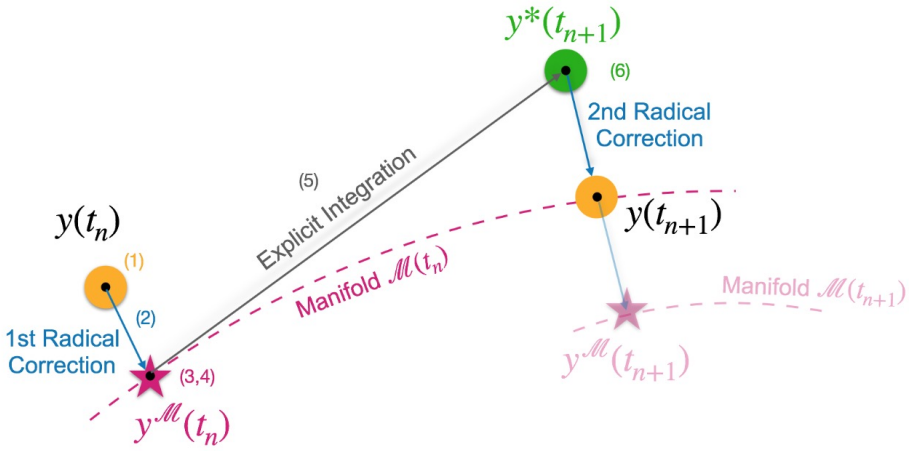

CSP solver algorithm with ANN

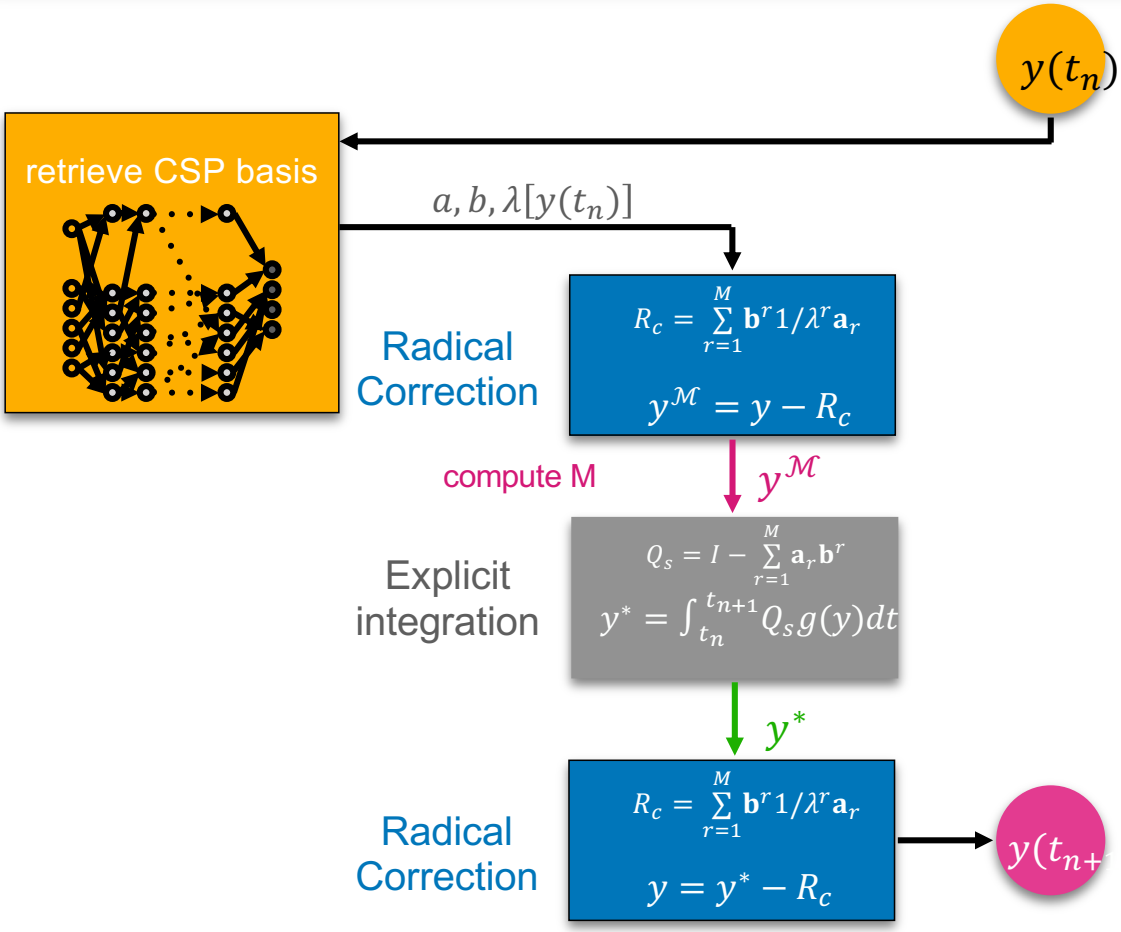

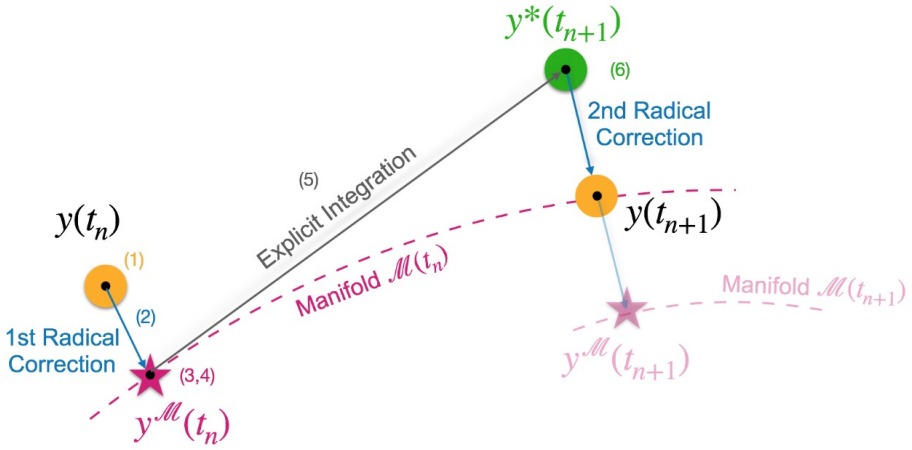

CSP solver algorithm with ANN

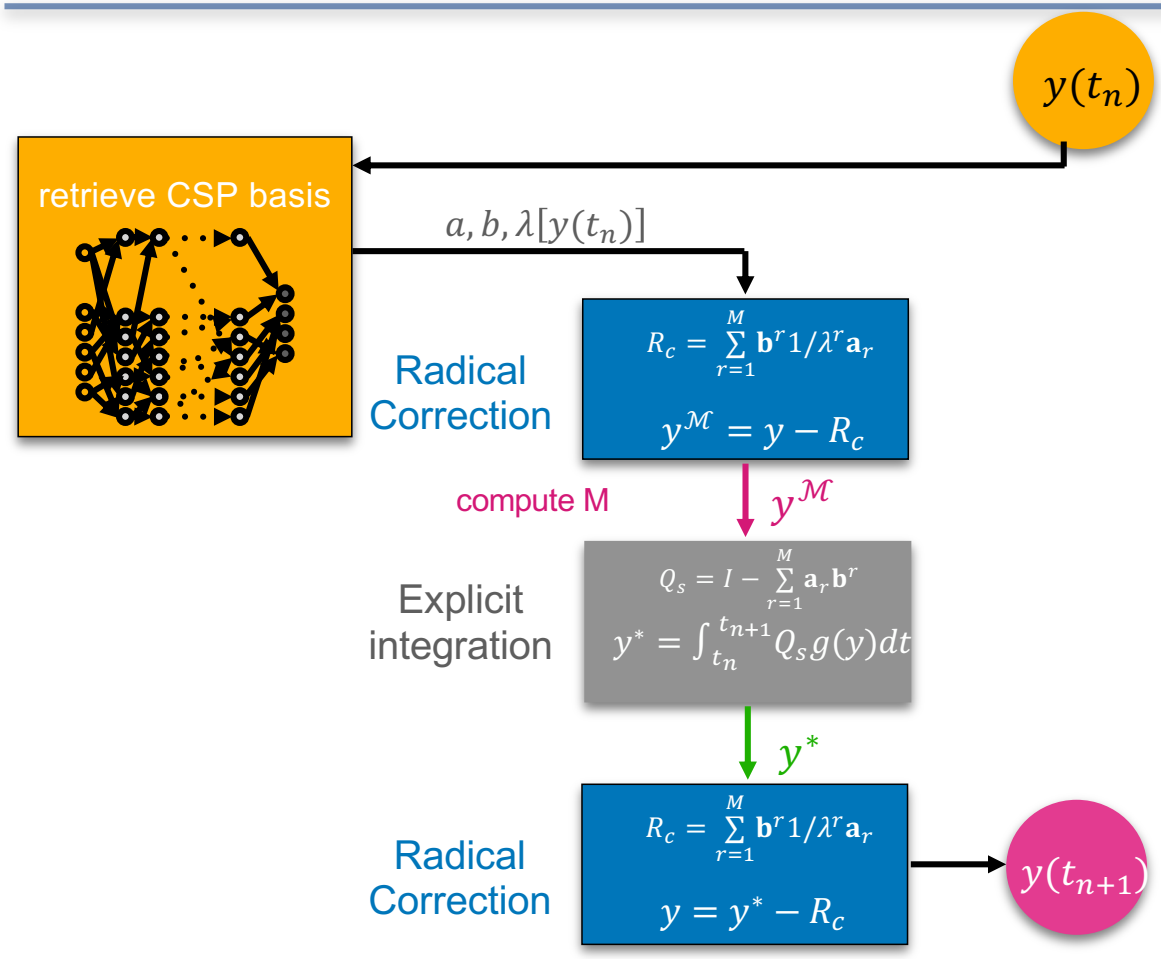

- **ANN** reconstructs the **projection basis**
  - Not the source term
  - Not the state at following time

  Physically informed construction
- Errors in ANN reconstruction are contamination of fast/slow scales
  - May affect performance
  - Don't affect accuracy

Solver accuracy

- Integration accuracy is very high
- Only the slow dynamics is resolved
- *M* represents the adaptivity (how many fast scales, locally)
- Timesteps are larger wrt CVODE

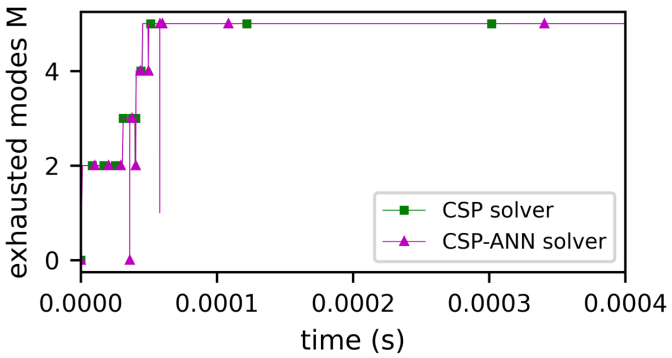

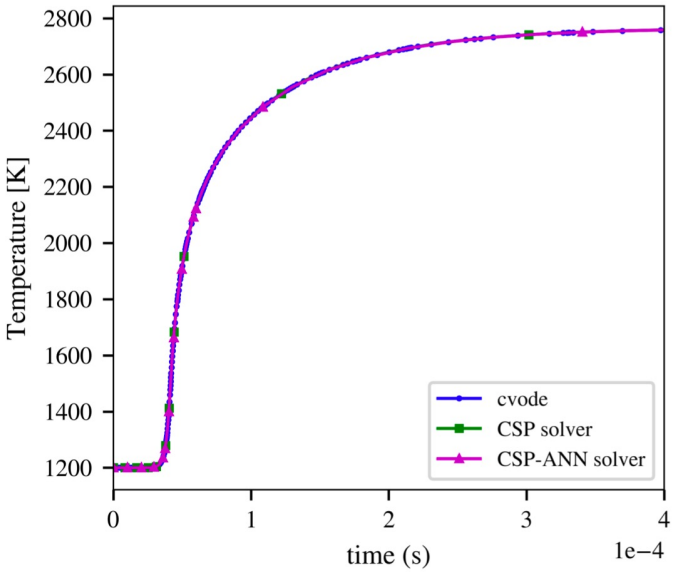

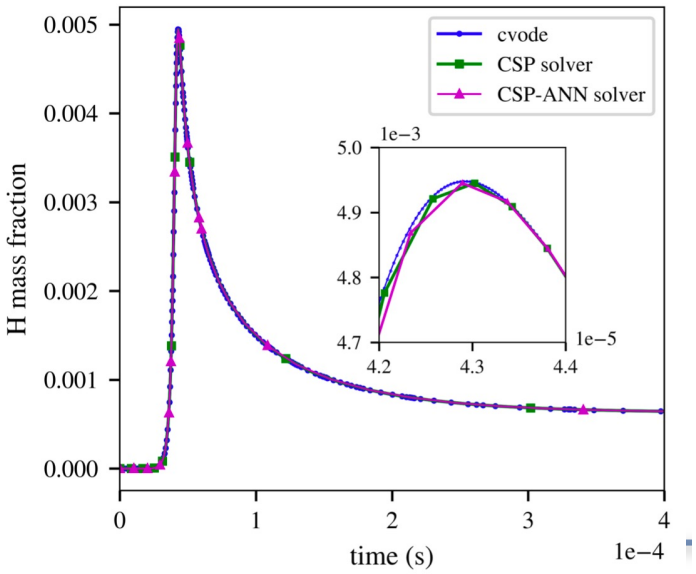

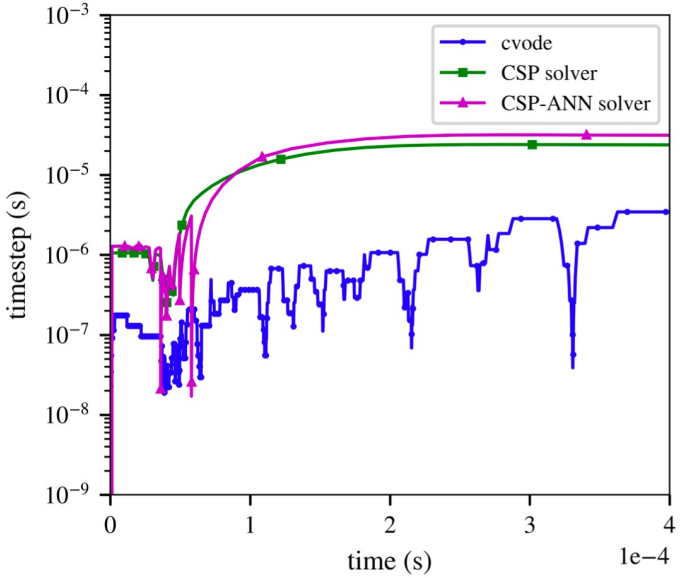

Summary

A significant speed-up was achieved by

- Matrix-based chemical source term evaluation on GPU
- MPI+CUDA with minimal memory copy

An intrusive ANN approach to accelerate the CSP solver

- The construction is robust to errors in basis prediction by ANN
- Integration accuracy is comparable to CVODE
- Slight performance improvements with a small mechanism (9-species)
- Larger savings are expected with larger mech and PDEs

شكراً

THANK YOU!